Chapter 5

Photophysical Properties of Two New Donor-Acceptor Conjugated Copolymers and Their Model Compounds: Applications in Polymer Light Emitting Diodes (PLEDs) and Polymer Photovoltaic Cells (PPCs)

S. Ayachi, A. Mabrouk, M. Bouachrine and K. Alimi

Additional information is available at the end of the chapter

http://dx.doi.org/10.5772/54254

1. Introduction

Organic semiconductors hold the combined properties of inorganic semiconductors such as silicon and more desirable properties of plastics [1,2]. Since, the inception of the field of plastic electronics, various organic semiconductors including conjugated polymers and small molecules have been synthesized, studied, and applied to optoelectronic semiconductor device structures in order to improve efficiency, reduce cost or realize new applications that are difficult to achieve with silicon-based technology [3,4].

Recently, the exploitation of polymer as an active layer in organic electronic displays has received a particular attention. In this direction, greater efforts have been devoted to seek new possibilities for use in optoelectronic devices such as Polymer Light Emitting Diodes (PLEDs) [5-11], Polymer Photovoltaic Cells (PPCs) [12-23] and Polymer Field Effect Transistors (PFET) [24-33]. The field of PLEDs is still an active research area since the first conjugated conducting or semiconducting polymeric material, poly(p-phenylene-vinylene) (PPV), was reported by Burroughes et al. in 1990 [34]. In fact, only polymers can enable manufacturing of large-area light-emitting displays. These electronic devices need special polymers with specific and adapted properties. Since then, there have been increasing interests and research activities in synthesis and design of new polymeric materials for organic electronic devices. However, their properties and those of the related devices are still poorly understood.

One of the requirements for efficient PLEDs is balanced charge injection from the two electrodes and efficient transport of both holes and electrons within luminescent layer in the device structure [35]. More recently, much effort has been devoted to develop wide band gap conjugated polymers for application in light emitting diodes. Then, a number of conjugated polymers including poly(p-phenylene-vinylene) (PPV) [36,37], poly(p-phenylene) (PPP) [38-41], polythiophene (PT) [42,43] and polyfluorene (PF) [44] have been widely used as light-emitting materials in devices. However, one major problem with these polymers is that they are π-excessive in nature and hence are much better at accepting and transporting holes than electrons. Another series of polymers containing π-deficient heterocycles like pyridine [45] and oxadiazoles [46] show greater tendency to transport electrons than holes [47].

To tune the emission properties of PLEDs, sophisticated control of the polymer luminescence color, efficiency, and charge transport properties are required. The emission wavelength depends on the extent of conjugation/delocalization, and can be controlled by the modification of the configuration or conformation of the polymer and by interactions with the local environment [48,49]. This can be achieved by grafting functional moieties such as electron donor or acceptor groups, which allow the modulation of the electronic structure of the conjugated backbone [50,51]. Donor–acceptor (D–A) organic molecules are among the most important conjugated polymers, that produce low bad gap useful in technological fields novel materials, by adjusting the HOMO and LUMO levels [52-54]. The low optical band gaps of the compounds should result by alternating the electron-rich unit of donor segments and the strong electron-deficient unit of acceptor segments in the structure. Then, superior transport properties in organic materials can be achieved with planar and highly conjugated chains [55-57]. Many investigations have proven that conjugated D-A type polymers play important roles in their balanced charge transporting properties and show unique optical properties. The HOMO and LUMO energy levels of these systems are important for understanding charge injection processes in the luminescent devices [58-60].

On the other hand, due to their interesting electrical, optical and optoelectronic properties, conjugated oligomers represent a prominent class of compounds from the viewpoint of theory, synthesis, and applications in materials science [61-65]. Moreover, they are model compounds for the corresponding polymers [66,67]. In parallel to recent experimental work on oligomers, theoretical efforts have also begun complementing the experimental studies in the characterization of the nature and the properties of their ground- and lowest electronic excited states [68-73]. In addition, these approaches have provided significant insight into the electronic and optical properties of conjugated polymers. In the absence of structural information, the experimental measurement, in conjunction with molecular orbital theory, is a valuable tool in analyzing the electronic structure of polymers. This enables an estimate not only of the relative energies of the electronic levels but also of their detailed distribution over the whole molecule. The ionization Potential (IP), electron affinity (EA), molecular electronic structure of the ground and lowest excited states as well as the nature of absorption and photoluminescence obtained through quantum calculations are of great interest prior to fabricating organic devices.

In this context, two new alternating donor-acceptor conjugated copolymers, both of which may be used in organic electronics, are investigated here. The first one is a copolymer containing thienylene-dioctyloxyphenyle-thienylene (TBT) and bipyridine (BIPY) units as shown in Fig. 1 that can be used as an active layer in PLEDs. It is constructed with dioctyloxy substituted phenylene incorporated between two electron-rich-thiophene units, abbreviated as TBT unit, and a bipyridine (BIPY) unit (Fig. 1). It was obtained by the Stille reaction method and the detailed synthesis procedures and characterization have already been reported [74,75]. The soluble copolymer has a well-defined structure and exhibits excellent optical properties. The number average (Mn) and weight average (Mw) molecular weights of the copolymer, determined by gel permeation chromatography (GPC) using polystyrene as standard, are obtained as 3098 and 3477, respectively. The corresponding polymerization degree, DPn, is found to be 5 corresponding to 25 cycles of number. Photophysical properties of copolymer including Raman scattering, UV-Visible optical absorption and emission are studied.

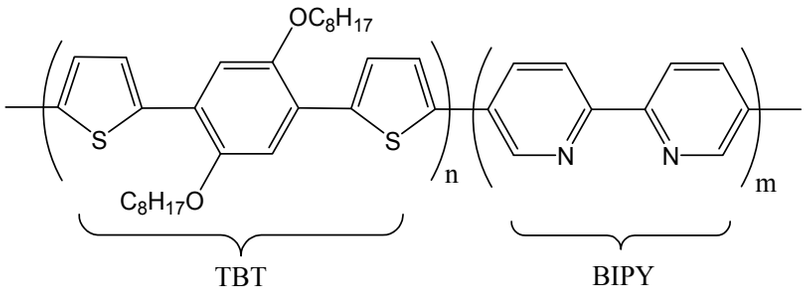

Figure 1. Chemical structure of TBT-BIPY copolymer.

Introducing long alkoxy pendants at 2 and 5 positions of the phenyl ring improves the solvent processability which is a prerequisite for fabricating organic light-emitting diodes (OLEDs) by the spin coating method.

The second part of this chapter concerns a composite based on Benzothiadiazole mixed with carbazole, or hexylthiophene that can be used for fabricating Polymer Solar Cells (PSCs). PSCs based on the bulk heterojunction (BHJ) structure have attracted broad attentions in recent years [76,77]. The requirements for the structure and properties of polymeric donors are low band gap, broad absorption range, high mobility and appropriate HOMO and LUMO levels [78]. Among the polymers tested for suitability as an active layer, poly(3-hexyl-thiophene) (P3HT) and poly(carbazole) (PCz) have emerged as promising candidates for applications in optoelectronic devices because of their exceptional properties [79,80]. However, alternative copolymers of [2,1,3]-benzothiadiazole (BT) acceptor units with various donor units have attracted particular attention for using them in high performance PSCs [81-83]. To optimize the material properties, conjugated polymers with alternating electron-rich and hole-rich units along their backbone have been extensively developed because their absorption spectra and band gap can be readily tuned by controlling the intramolecular charge transfer (ICT) from donors to acceptors [84].

However, in these linear D-A polymers, the molecular interactions and packing orientation of the conjugating moieties need to be carefully controlled to ensure proper process ability

and charge transporting properties [85]. A fundamental understanding of the ultimate relations between structure and properties of these materials is necessary for using them in photovoltaic cells. A number of studies demonstrate that the interplay between theory and experiment is very important in providing useful insights in understanding the molecular electronic structure of the ground and excited states as well as the nature of absorption and photoluminescence [86]. To rationalize our theoretical results, the simulated data are compared with the available experimental data [87].

In what follows, we elucidate the photophysical properties of the benzothiadiazole derivative compounds with structures as shown in Fig. 2 (a,b). These two D-A polymers provide a basis for a more comprehensive study of the backbone ring, heteroatom and fused ring effects on polymer properties. Therefore, it is of practical significance to extend our previous work to a comprehensive theoretical investigation on these two types of BTD-based derivatives. Moreover, poly(3-hexyl-thiophene) (P3HT) units have relative higher charge mobility in comparison with other conjugated polymers and have been widely used as π-conjugating spacers [88,89]. Its insertion in the polymer backbone serves the dual purpose of transporting carriers and providing sites for exciton dissociation [90]. Moreover, the incorporation of electron-withdrawing moieties (3HT) as side chains leads to some useful properties which can further widen the absorption spectrum.

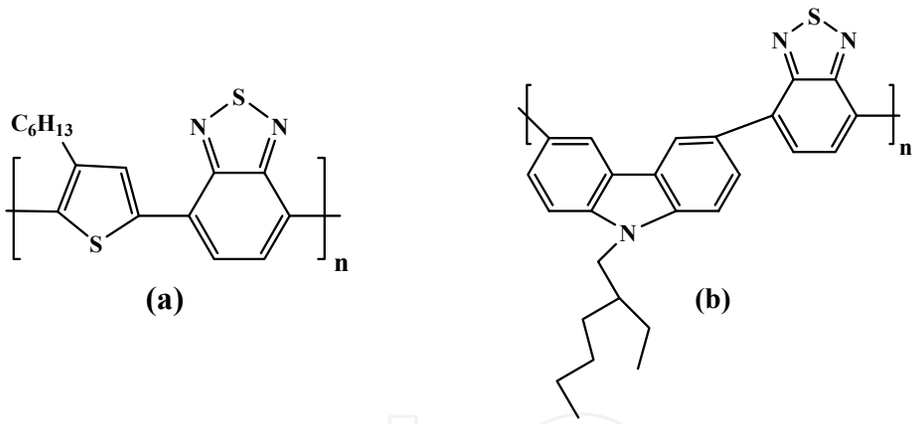

Figure 2. Chemical structure of compounds under study: (a): P3HTBT, (b): PCzBT.

Recently, the conjugated P3HT2BTCz compound, built as carbazole-thiophene-benzothiadiazole, has been copolymerized onto the backbone of the copolymer as shown in Fig. 3. This compound has been synthesized and experimentally characterized, using only photoluminescence and optical absorption spectroscopy. Their related intense and broad absorption bands as well as favorable excited-state energy levels make them good candidates for fabricating PSCs. Thus, if P3HT2BTCz compound is blended with [6,6]-phenyl-C_{61}-bytric acid methyl ester (PCBM) fullerene derivative into BHJ photovoltaic devices [87], then the conversion efficiency may be increased.

Here further investigations of geometrical parameters, electronic structures, photo-physical and vibrational properties of these compounds are carried out, on the basis of quantum-chemical calculations, providing a reasonable interpretation of the experimental results and

better understanding of the relationship between the structure and resulting properties. Finally, the parameters that influence the photovoltaic efficiency are elucidated. We think that the presented study of structural, electronic, optical, and charge transfer properties for this compound will help the design more efficient functional photovoltaic copolymers.

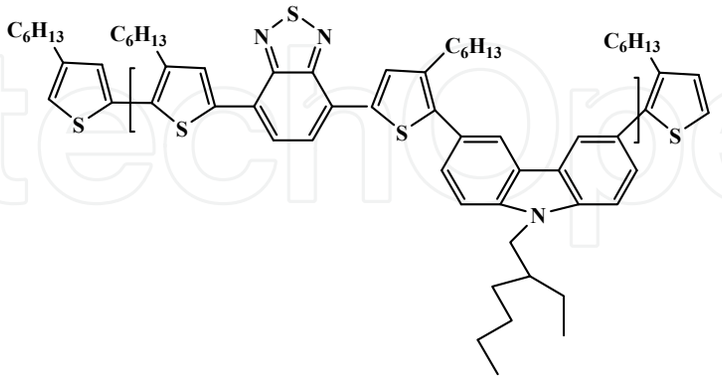

Figure 3. Chemical structure of P3HT2BTCz compound.

The objective of the presented result here is not to develop or optimize any applications, but to understand why and how the combined theoretical and experimental studies on copolymers can be conducted in developing optimized Polymer Light Emitting Diodes (PLEDs) and Photovoltaic Cells (PPCs).

2. Theoretical methodology

All molecular calculations are performed in the gas phase using Density Functional Theory (DFT) implemented in the GAUSSIAN (03) program [91]. We have used the B3LYP (Becke three-parameter Lee-Yang-Parr) exchange correlation functional [92,93] with 3-21G* and 6-31G* as basis sets. In the first part, the calculation of conformational characteristics has been done by varying the torsion angle in steps of 20° from $\theta = 0°$ to $\theta = 180°$. For each increment, the dihedral angle is held fixed while the remainder of the molecule is optimized. The energy differences in electronic states are always calculated relative to the corresponding absolute minimum conformation and then the relative potential energy surfaces are drawn.

In the optimization procedure of these compounds, the alkyl chains at the N-9 positions of carbazole (Cz) motifs and dioctyloxy groups in TBT-BIPY copolymer are replaced by methyl and methoxy groups, respectively. This has been proven that the presence of alkyl/alkoxy groups does not significantly affect the equilibrium geometry and hence the electronic and the optical properties [94]. Hexyl groups in 3HT motifs are then replaced by methyl groups. The optimization of the composite (P3HT2BTCz: PCBM) is done in two steps. First optimization with PM3 semi-empirical method was carried out, then the resulting structure was re-optimized by DFT/B3LYP/3-21G* to find the equilibrium geometrical structure.

Optical absorption spectra are calculated using the Time-Dependant Density Functional Theory (TDDFT) [95] based on optimized ground state geometries [96]. Theoretically the transition energies and their respective intensities in a given configuration interaction (CI)

expansion of singly excited determinants are determined [97]. The electronic configurations for the lowest 50 singlet-singlet transitions are obtained using the same basis set. Then, the obtained data are transformed using the SWizard program [98] into simulated spectra as described in the literature [99]. Finally, the nature and the energy of vertical electron transitions (the main singlet-singlet electron transitions with highest oscillator strengths) of molecular orbital wave functions are presented. The photoluminescence (PL) spectrum has been derived from CIS/TDDFT calculation [100]. Similar procedures are applied on TBT-BIPY model compound on the basis of ground and lowest singlet excited-states, but with two additional methods (CIS/3-21G* and the semi-empirical quantum-chemical ZINDO levels) for absorption and emission properties [101]. The vibrational properties as well as force constants are also examined through results derived from the Molecular Orbital Package (MOPAC 2000) [102].

3. Part I: TBT-BIPY copolymer for Light Emitting Diodes (PLEDs)

3.1. Raman scattering spectroscopy

The Raman spectrum recorded for the excitation line of 1064 nm is presented in Fig. 4a. We have found that the Raman spectrum is dominated by bands originating from the thiophene, the di-alkoxy-substituted phenylene and pyridine rings vibration. According to the literature [103,104], the major band in the spectrum can be attributed to C_α=C_β stretching vibration of the thienyl ring at roughly 1444 cm^{-1} and the relatively weaker band at about 1604 cm^{-1} can be assigned to the C=C stretching vibration of the phenylene ring. The 1302 cm^{-1} can be attributed to the interring $C_{thienyl}$-C_{phenyl} vibration. In addition, we notice a strong asymmetry in intensity of the dominant triplet, occurring at 1444, 1543 and 1604 cm^{-1}, resulting from the short conjugation length of the material [105].

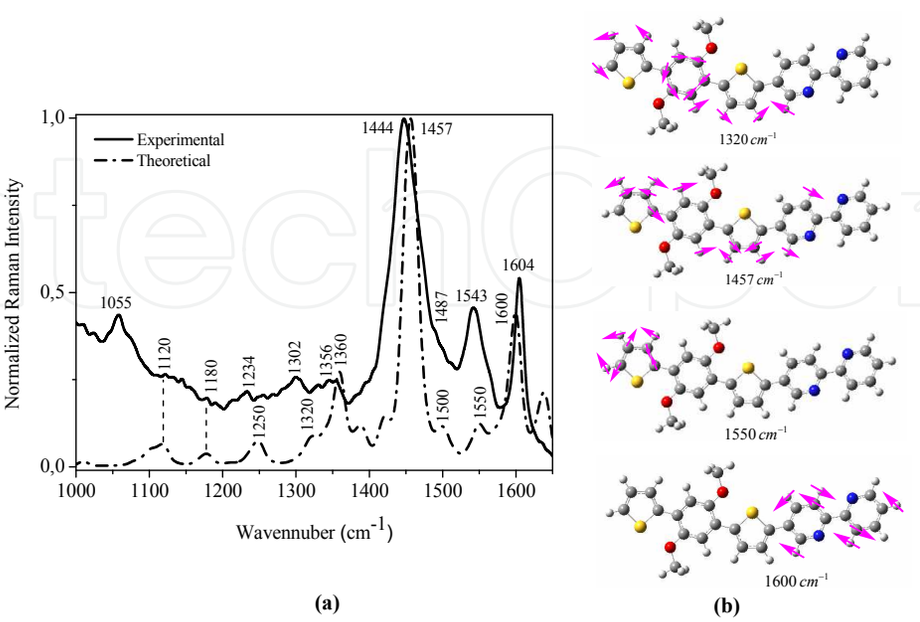

Figure 4. (a) Experimental and theoretical normalized Raman spectra and (b) Selected Raman vibrational modes of the calculated frequencies of TBT-BIPY copolymer.

3.2. Optical absorption and emission properties

The optical properties of the copolymer were studied, in chloroform solution and recorded at ambient temperature, by using UV-Vis and fluorescence emission spectroscopies (Fig. 5). The TBT-BIPY solution showed a sharp peak absorption maximum at 436 nm corresponding to the $\pi \rightarrow \pi^*$ electronic transition in the polymer backbone. This band appears at 517 nm for the polymer film. Obviously, the red shift of about 79 nm in the film state is due to the π-π* stacking effect [106]. The optical band gap, defined by the onset absorption of the polymer in the chloroform solution state is 2.43 eV. The polymer showed low band gap when compared to that of TBT-BIPH (2.48 eV). This may be due to the strong interaction between electron acceptor (TBT) and strong electron acceptor segments (BIPY) in the polymer backbone. Then, this optical band gap of the copolymer could be attributed to the D-A structure of polymer matrix.

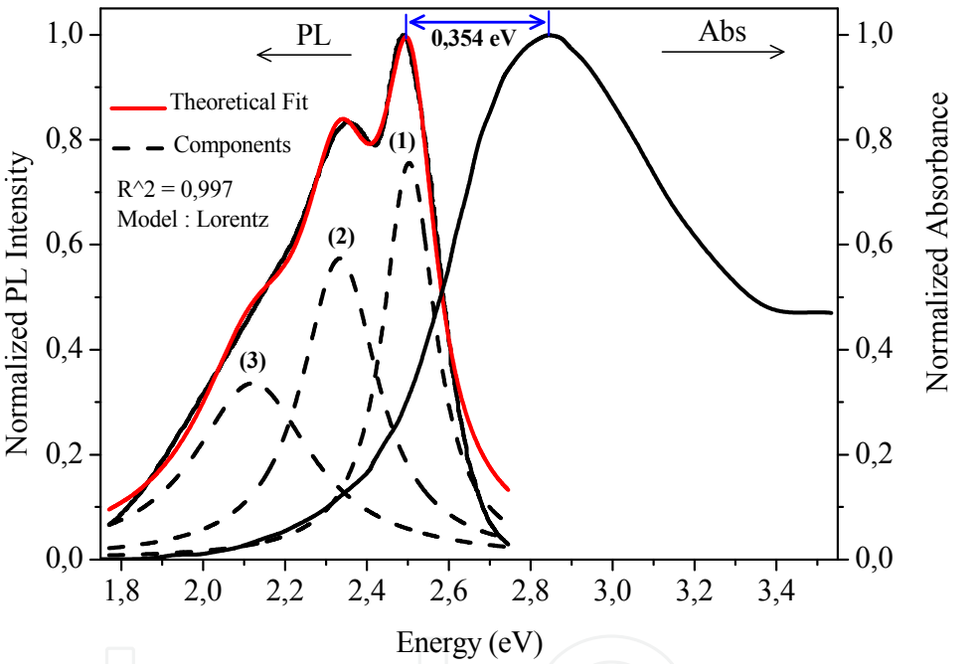

Figure 5. Normalized optical absorption and photoluminescence spectra of TBT-BIPY copolymer. The PL deconvolution spectrum was given in the same figure.

Fig. 5 includes also the fluorescence spectrum of copolymer that gives a bright blue-greenish fluorescence with the maximum emission wavelength of 498 nm with the excitation wavelength at 450 nm in chloroform solution state. This emission is corresponding to the onset of $\pi \rightarrow \pi^*$ transition of the electronic absorption spectra. The band gap of the polymer (2.43 eV) estimated from the onset position of the absorption (510 nm) essentially agrees with the λ_{max} value (498 nm, 2.48 eV) of the main fluorescence peak, indicating that the fluorescence takes places by migration of electrons in the conducting band to the valence band. It is worthy to note that the PL spectrum of the compound shows well-resolved structural features with maxima at 498, 527 and shoulder at about 580 nm assigned to the 0–0, 0–1, and 0–2 intra-chain singlet transition, respectively (the 0–0 transition, the most

intense) [107]. The stocks shift was found to be 62 nm (0.35 eV). This shift points to large structural differences between the ground and excited states in the material. In addition, from PL deconvolution spectrum, it should be noted that the energy difference (~ 0.18 eV) agrees well with that of the most intense Raman vibration modes at around 1450 cm^{-1}.

3.3. Theoretical part

3.3.1. Conformational analysis

In the absence of structural information, we have assumed that the oligomer tends to be planar because of two reasons: (i) interchain interactions (packing force) tend to significantly reduce the torsion angles between adjacent units in the solid state and (ii) electronic and optical properties are weakly affected by small changes in torsional angels. To determine the minimum energy configuration, we perform fully geometrical optimizations on TBT-BIPY with B3LYP/3-21G*. Since there is only one type of substitution on the phenyl ring (substitution 2 is equivalent to the site 5), three different conformation types can occur in TBT-BIPY copolymer structure. The potential energy surface (PES) of copolymer is obtained by partial optimization as shown in Fig. 6.

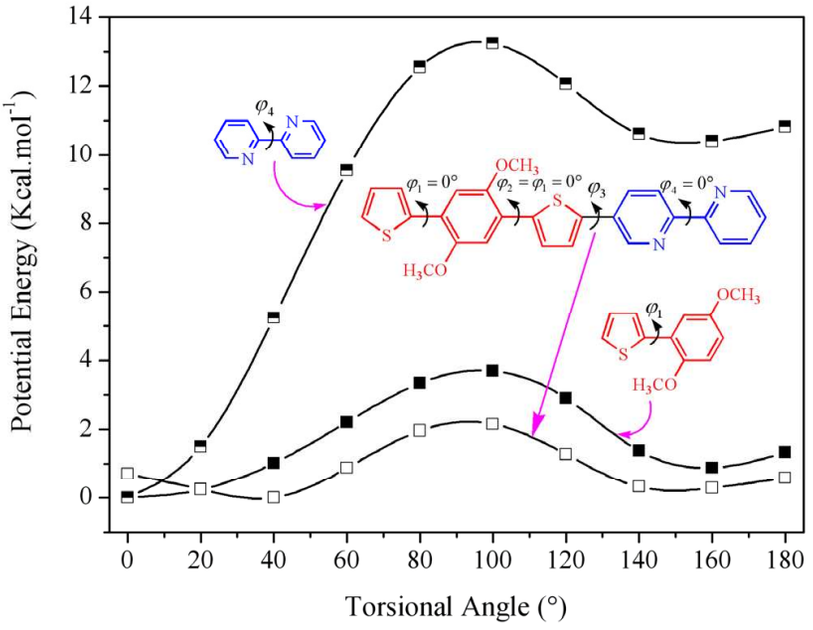

Figure 6. Potential energy curves of thienylene-2,5-di-methoxy-phenylene, BIPY and TBT-BIPY obtained from DFT/B3LYP/3-21G* level of theory.

As these structures show flexibility in the molecule, first of all, individual torsion potentials for the two structures of thiophene-di-methoxy-phenylene (TDMP) and bipyridine (BIPY) are obtained for each molecule as a function of the inter-ring C-C dihedral angle ϕ_1 (torsional angle between the thiophene and di-methoxy-phenylene rings) and ϕ_4 (torsional angle between the two pyridine rings) by varying them from 0° (syn-planar) to 180° (anti-planar) in steps of 20°. Therefore, to construct the potential energy curve for TBT-BIPY

copolymer, ϕ_1 and ϕ_4 are held fixed and the torsional angle ϕ_3 (dihedral angle between the thiophene and pyridine rings) is calculated in the same way by varying the torsional angles (ϕ_1 and ϕ_4) as described above. From the conformational analysis of TDMP and BIPY, it is found that both show a minimum at the torsional angle around 0°, and they adopt co-planar conformations. However, when BIPY is connected to TBT unit, molecules get twisted out of the planarity with an angle $\phi 3 = 40°$. Accordingly, all the inter-ring dihedral angles are kept constant at $\phi_1 = \phi_2 = \phi_4 = 0°$ and $\phi_3 = 40°$ during the geometry optimizations.

3.3.2. Ground- and excited-state structures

The optimized structure of TBT-BIPY optimized using DFT//B3LYP/3-21G* is shown Fig. 7. The selected bond lengths and twist angles are collected in Table 1.

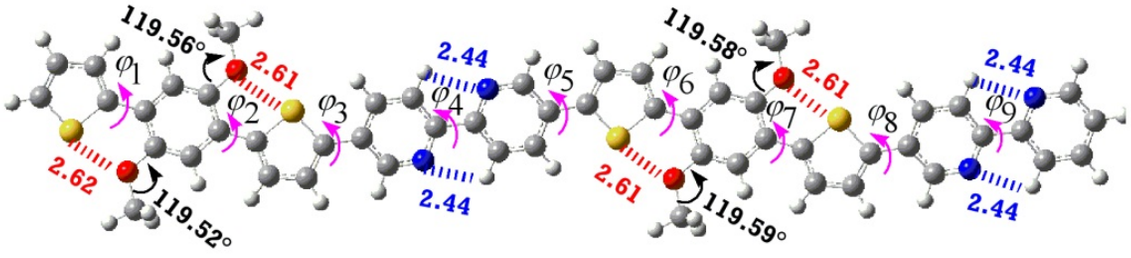

Figure 7. Ground state B3LYP/3-21G* optimized structure of 2-TBT-BIPY copolymer. The values written in red (blue) color represent S--O (N--H) distances in Angstrom. φ_n (n=1-9) represents the dihedral angle between rings and the values expressed in degree are the C-O-C angles.

As shown in Table 1, the two TBT and bipyrdine units of 2-TBT-BIPY adopt planar conformations with dihedral angles inferior to 1°. Whereas, the dihedral angles φ_3, φ_5 and φ_8 for 2-TBT-BIPY are twisted out of plane of ~24°. In addition, the C-O-C angles are not affected along the polymer chains and are evaluated to be 119.5°.

Dihedral Angle (°)	Ground State	Excited State
φ_1	-0.28	-0.21
φ_2	-0.39	-0.31
φ_3	23.61	20.31
φ_4	0.007	-0.72
φ_5	-24.52	-2.42
φ_6	-0.20	-0.34
φ_7	-0.55	-0.41
φ_8	23.86	1.85
φ_9	-0.088	-0.091

Table 1. Calculated dihedral angles in their ground- and excited-states of 2-TBT-BIPY copolymer.

It is worth noting that the interaction forces between the oxygen atom (negatively charged) and the sulfur atom (positively charged) in the TBT unit are attractive [108-110]. Similar results are found for the Bipyridine unit; in which intra-molecular interaction occurs between non-bonded nitrogen and hydrogen atoms (the atomic charges are listed in Table 2 referred to the individual atoms in the numbering sequence shown Fig. 8). In fact, the calculated bond lengths of S--O (N--H) bonds are found to be ~2.62 Å (~2.44 Å), which correspond to ~79% (~92%) of the sum of their Van der Waals radii, fall inside the Van der Waals contact distance of the S--O (3.32 Å) and N--H (2.64 Å) and outside of their covalent contacts of 1.70 Å for S-O and 0.91 Å for N-H. In this case, the planar conformations are stabilized by the non-bonded S--O and N--H interactions [111].

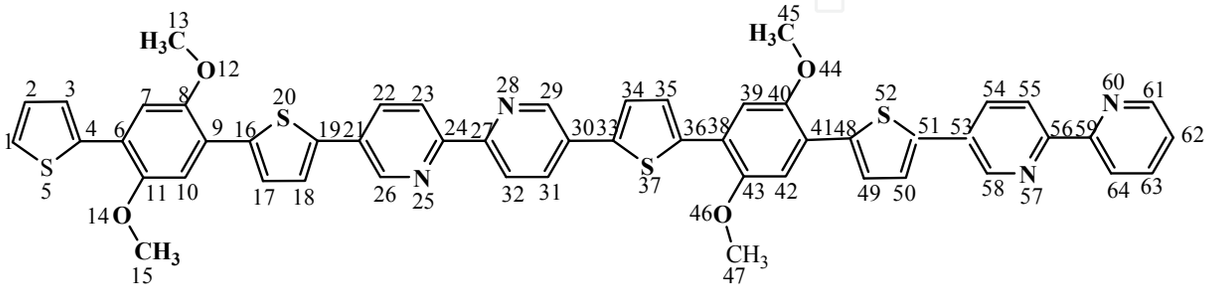

Figure 8. 2-TBT-BIPY copolymer structure with individual atoms in the numbering sequence.

	Atomic charges (e)	
Atoms	Ground State	Excited State
S_5/O_{14}	0,459/-0,565	0,513/-0,757
S_{20}/O_{12}	0,492/-0,566	0,560/-0,759
N_{25}/H	-0,619/0,220	-0,764/0,287
N_{28}/H	-0,619/0,219	-0,767/0,287
S_{37}/O_{46}	0,494/-0,565	0,568/-0,760
S_{52}/O_{44}	0,494/-0,565	0,569/-0,760
N_{57}/H	-0,618/0,220	-0,767/0,286
N_{60}/H	-0,605/0,221	-0,753/0,288

Table 2. Atomic charges of sulfur, oxygen, nitrogen and hydrogen atoms in S--O and N--H intra-molecular interactions.

Further, the highest occupied molecular orbital (HOMO), lowest unoccupied molecular orbital (LUMO) as well as the HOMO-LUMO energy gap ($\Delta_{LUMO-HOMO}$) are studied. Accordingly, for 2-TBT-BIPY, the HOMO is at -4.922 eV, LUMO at -2,152 eV and the energy difference between these levels is thus 2.77 eV. To further understand the optical property changes, Fig.9 illustrates the three highest occupied and three lowest unoccupied orbital levels for the 2-TBT-BIPY copolymer.

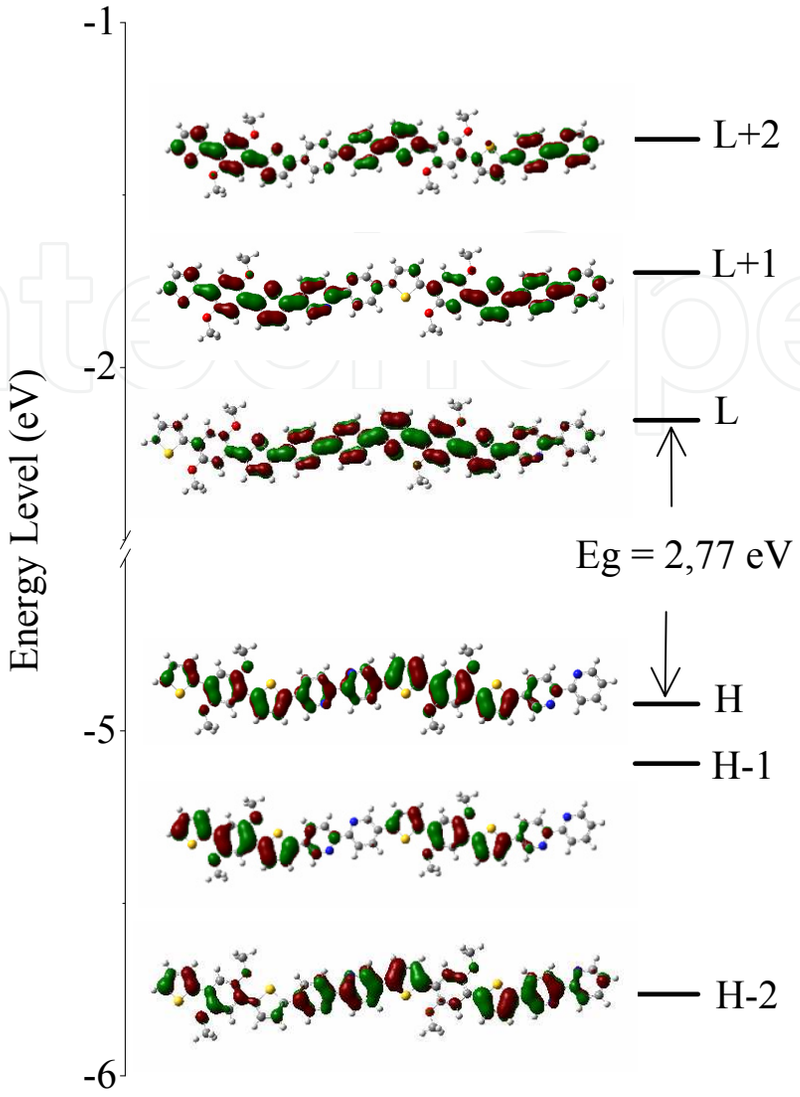

Figure 9. The DFT//B3LYP/3-21G* calculated energy levels for 2-TBT-BIPY copolymer.

The vibrational Raman frequencies are calculated using the same method on geometry-optimized structure and are directly compared to those obtained from the Raman spectroscopy measurements. In Fig. 4a, we have plotted the normalized theoretical and experimental Raman spectra of the TBT-BIPY copolymer compound. It is relevant to note here that the vibrational spectrum calculated by DFT methodology agree satisfactorily with the experimental spectrum both in relative intensities and peak positions. The deviation between the measured Raman scattering and theoretically vibrational frequencies are less than 30 cm^{-1}. Moreover, it was found that there were no negative vibrational frequencies, which indicate that optimized structure was at the energy minimum. This implies that the theoretically determined structure of copolymer is the most accurate description of the electronic structure. Accordingly, the experimental and calculated Raman bands at 1444 and 1457 cm^{-1}, respectively, assigned to the thiophene ring vibrations [103-104], are strongly resonant with the $\pi \rightarrow \pi^*$ electronic transition of compound. The most important Raman vibrational modes are shown in Fig.4b.

By combining the experimental data (optical band gap and Raman frequencies) with DFT calculations, two units of TBT-BIPY copolymer were considered as model structure for predicting the optical and emission properties.

For better understanding of the optical and emission processes, we have firstly computed the bond lengths of the ground and excited states, where the changes of bond lengths can be compared. The values of bond lengths for the 2-TBT-BIPY copolymer, in their ground- and excited-states are shown in Fig. 10. It can be seen that some bond lengths increase and some decrease in the excited state. Furthermore, we find that all the bond lengths of two bipyridine as well as those of C-O-C are shortened. Whereas, in the left TBT unit, the C-C single bond of thiophene rings as well as that connecting the thiophene ring to phenylene and bipyridine rings increase. In addition, in the second TBT unit, double bonds of thiophene rings and single/double bonds of substituted phenylene rings also increase.

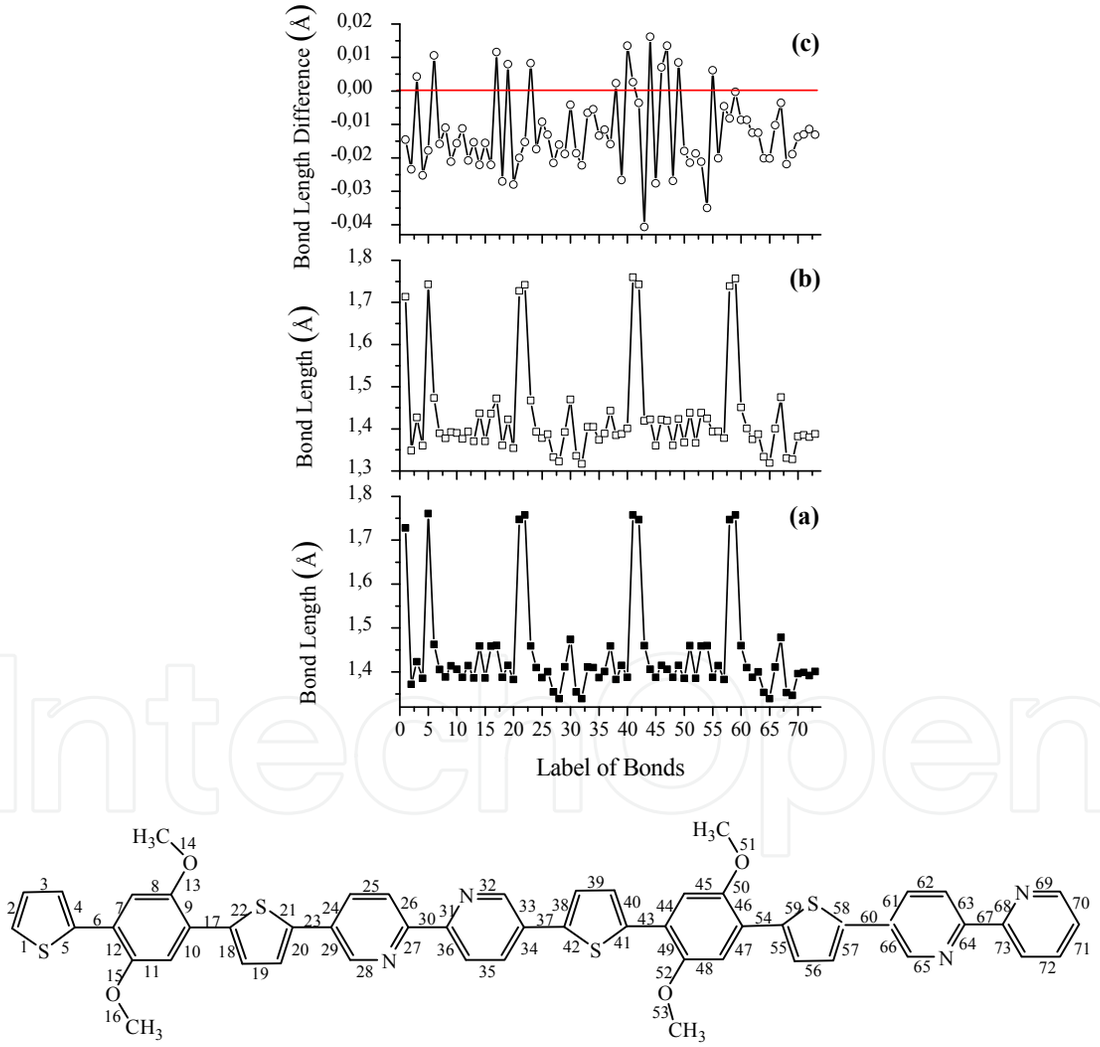

Figure 10. Bond length variation of ground (a) and excited (b) states of 2-TBT-BIPY copolymer as well as the difference in bond length between the excited and ground states (in Å) (c). The horizontal axis labels represent the bonds between adjacent atoms in the numbering sequence shown in Figure from the bottom.

On the other hand and whatever the state is, the non-bonded S--O and N--H contacts were found to be considerably shorter than the sum of their Van der Waals radii. These distances vary from ~2.62 Å to ~2.64 Å (S--O) and from ~2.43 Å to ~2.46 Å (N--H), when excited from the ground to excited states, which confirm the occurrence of non-covalent intra-molecular interactions. We believe that attractive interaction forces can modify the C-O-C angles in the excited state. This indicates that the singlet excited state should be much more planar than their ground state.

3.3.3. Electronic transitions

We have applied a variety of theoretical approaches, including CIS/3-21G*, TD-B3LYP/3-21G* and ZINDO methods to study the optical and emission properties of TBT-BIPY copolymers. The theoretical results thus obtained are compared with the experimental ones. All the energy levels calculated using the Time Dependent Density Functional Theory (TD-DFT), the CIS/3-21G* and the semi-empirical quantum-chemical ZINDO are used to predict the optical absorption and emission spectra of the ground (S_0) and first excited (S_1) optimized structures. The assignment of electronic transitions and their oscillator strengths are also calculated using these three methods.

From theoretical calculations, the wavelength of transitions from the ground to the first excited state ($S_0 \rightarrow S_1$) and from the first excited state to ground state ($S_1 \rightarrow S_0$) having the largest oscillator strength as well as their corresponding molecular orbital character for 2-TBT-BIPY are listed in Table 3. The corresponding experimental optical absorption and emission wavelengths measured in TBT-BIPY copolymer in chloroform solution are also listed in the same table. Clarke et al [112] suggest that the importance of the HOMO-LUMO transition may be easily understood from the spectral distribution of molecular orbitals. Accordingly, to a first approximation, a significant overlap found between HOMO and LUMO implies an intense transition between HOMO to LUMO and vice-versa. Here, the vertical $S_0 \rightarrow S_1$ transition dominates the H→L excitation by 60-81%.

Method of calculation	Optical absorption properties of ground state ($S_0 \rightarrow S_1$)				Emission properties of excited state ($S_1 \rightarrow S_0$)				Stokes shift (nm/eV)
	λmax (nm)	f	MO/Character	Coefficient (%)	λmax (nm)	f	MO/Character	Coefficient (%)	
CIS	357.2	4.364	H→L	60	398.7	3.055	L→ H	80	41.5
			H-1→L+1	22			L+2→H-2	5	(0.36)
			H-2→L+2	9					
TD-DFT	481.6	2.943	H→L	78	508.8	3.224	L→ H	82	27.2 (0.13)
ZINDO	439.4	3.781	H→L	81	519.2	4.352	L→ H	89	79.8
			H-1→L+1	5					(0.43)
Exp	436 nm				498-527 nm				62 (0.35)

(H=HOMO, L=LUMO, L+1=LUMO+1, etc.), f: Oscillator strength

Table 3. The vertical transition energies (nm) and their oscillator strengths of absorption from the ground to the first excited state ($S_0 \rightarrow S_1$) and emission from the first excited to ground ($S_1 \rightarrow S_0$) states of TBT-BIPY copolymers calculated by CIS/3-21G*, TD//B3LYP/3-21G* and ZINDO methods.

3.3.4. Frontier molecular orbitals (HOMO and LUMO)

To gain insight into the excitation properties and the ability of electron or hole transport, we have shown in Fig. 11 HOMO and LUMO together known as frontier molecular orbitals which contribute significantly to the electronic transitions between the ground and excited states in 2-TBT-BIPY.

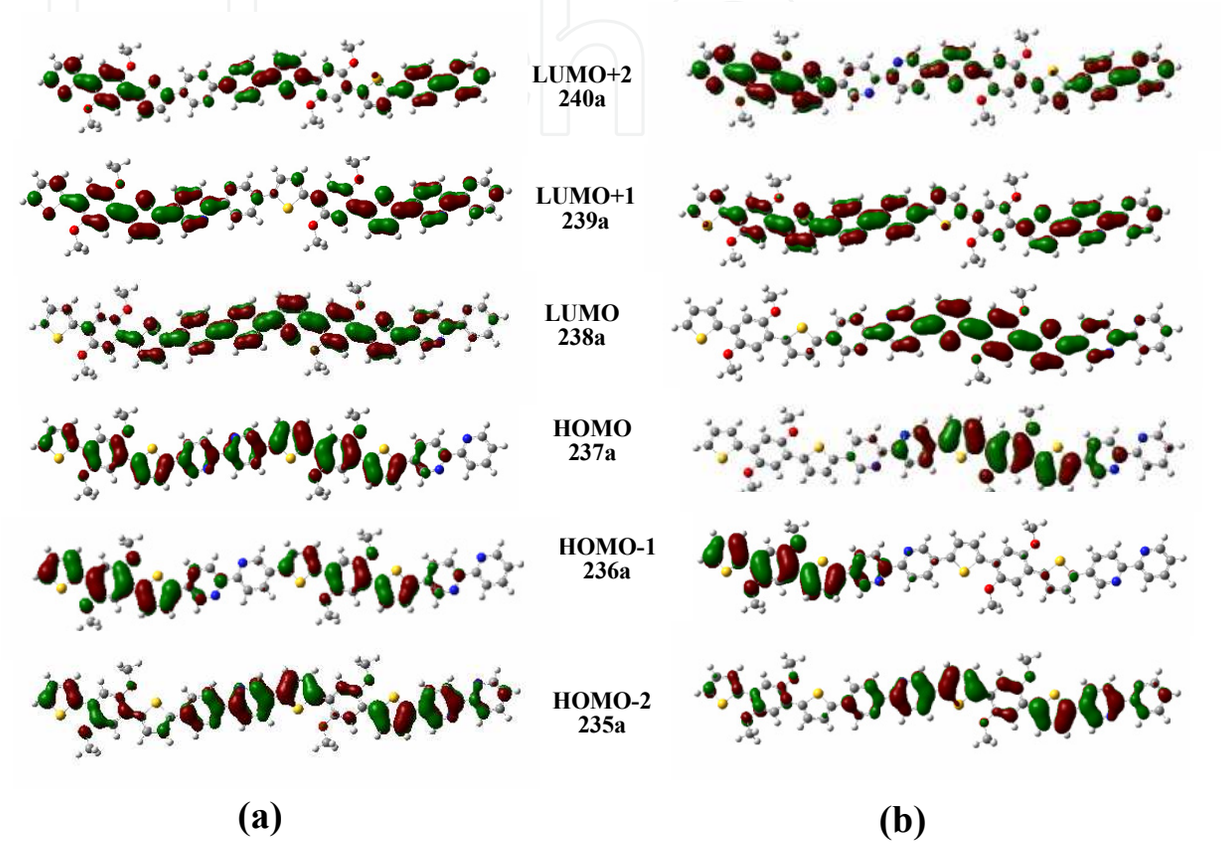

Figure 11. Contour plots for the HOMO and LUMO molecular orbitals which contribute significantly to the electronic transitions in 2-TBT-BIPY copolymers: (a) absorption from ground to excited and (b) emission from excited-to ground states.

We have examined and found that the presence of methoxy side chain does not have a significant effect on the molecular orbital distribution. In the HOMO, the C=C segments are π-bonding and have anti-bonding character with respect to their neighboring C=C units. Whereas, in the case of LUMO, the C=C units are anti-bonding and bonding in the bridge single bond. In general, excitation of a π-electron from HOMO to LUMO leads to increase the localization of electron density on the acceptor part of the molecule. Here, the promotion of one electron from HOMO to LUMO is explained by the frontier molecular orbital. For the TBT-BIPY copolymer, the LUMO favors the inter-ring mobility of electrons, while the HOMO only promotes the intra-ring mobility of electrons [116]. As outlined before, in the excited state of copolymer, both the HOMO and LUMO frontier molecular orbitals topology are significantly affected, particularly in the left TBT unit indicating their contribution to the excitation processes. In fact, in the ground state, the spatial distribution of the molecular

orbitals is rather delocalized over the molecule. Changing to the excited state geometry, they become more localized.

3.3.5. Mulliken charge distribution for TBT-BIPY

A schematic representation for the intra-molecular charge transfer (CT) in the ground and excited states of 2-TBT-BIPYcopolymer, calculated as the average of the summation of Mulliken charge distribution of the TBT and BIPY units, is displayed in Fig.12. In general, intra-molecular charge transfer is generated through the alternating donor-acceptor conjugated systems [117]. From this figure, we think that the alternating TBT (positively charged) and BIPY (negatively charged) can be used as donor and acceptor, respectively. We have separately examined their HOMO and LUMO levels, which indicates that for the TBT unit, the HOMO is at -4.29 eV and the LUMO at -1,29 eV and for bipyridine unit we get -6.52 eV for the HOMO and -1.33 eV for the LUMO. Although the LUMO levels for both are quite similar, a weak intra-molecular charge transfer in these molecules can established. Based on the comparison between ground and excited-state geometries for 2-TBT-BIPY, we deduce that the charge distributions are predominantly restricted to the substituted phenylene and thiophene units.

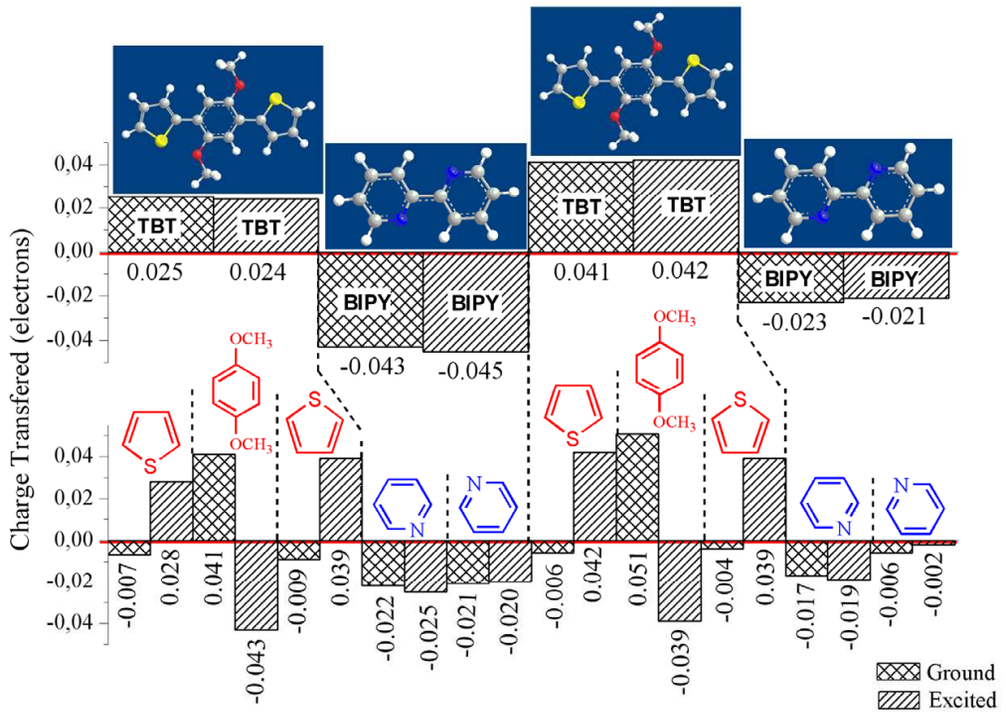

Figure 12. Illustration of the 2-TBT-BIPY copolymer structure with Mulliken charges distributions for TBT and BIPY units at the ground and excited states. All segments presented with dotted line separate the sub-units involved in the copolymer structure.

We can also predict the geometrical structure changes between the ground (S_0) and singlet excited (S_1) from the molecular orbitals. Therefore, to better understand the excitation

process in TBT-BIPY copolymer, we have investigated the molecular orbitals involved in the electronic transition.

3.3.6. Simulated optical and emission spectra for TBT-BIPY copolymer

In Fig.13, we have depicted the simulated results of the optical absorption and emission spectra for 2-TBT-BIPY copolymer using the above three methods. To select the accurate method for predicting these optical properties, we show the potential energy surface (PES) of the ground (U_g) and excited (U_e) states along with their normal coordinates for 2-TBT-BIPY copolymer in Fig. 14 and Table 4. In Fig. 14, the two potential energies surfaces (PES) are plotted along with their normal coordinate q and the absorption and fluorescence spectra obtained from the transition between these two PES, using CIS/3-21G* and TD-DFT, respectively. The optical absorption energy (E_{VA}), emission energy (E_{VE}) and the relaxation energy (E_R^{GS}, E_R^{ES}) are presented in Table 5. The Stokes shift (SS), which is defined as the difference between the absorption and emission energies (E_{VA}-E_{VE}), is usually related with the band widths of both the absorption and emission bands [118] and it is a measure of the energy loss due to the molecular relaxation. It can be expressed as: $SS = E_R^{GS} + E_R^{ES} = E_{VA} - E_{VE}$. From the results given in table 5, we show that the SS calculated by CIS/3-21 G* is about two times higher than that calculated by TD-DFT. Accordingly, due to the neglect of the effects of electron correlation and higher order excitations, the geometrical relaxation after the excitation contributes much to the Stokes shift calculated by CIS/3-21 G*. It is well known that the absorption energy (E_{VA}) is usually considered to be maximum in the absorption spectrum, but it must be corrected for the zero-point vibrational energy (ZPE). In our case, compared with the results given in Table 4, SS energies calculated by CIS/3-21G* and TD-DFT methods as given in Table 5 deviate only by 0.084 eV and 0.088 eV, respectively. This difference of about 0.08 eV probably represents the value that needs to be used to correct the theoretical data. By such correction to the experimental value an excellent agreement is obtained with the result calculated by ZINDO method as shown in Table 4 for 2-TBT-BIPY copolymer.

	CIS/3-21G*	TD//B3LYP/3-21G*
E_{VA} (eV)	7.613	2.899
E_{VE} (eV)	7.169	2.681
E_R^{GS}(eV)	0.25	0.099
E_R^{ES}(eV)	0.194	0.119
SS (eV)	0.444	0.218

Table 4. The optical absorption energy (E_{VA}), emission energy (E_{VE}), relaxation energy (E_R^{GS}, E_R^{ES}) and Stokes shift (SS) calculated by CIS/3-21G* and TD//B3LYP/3-21G* methods for 2-TBT-BIPY.

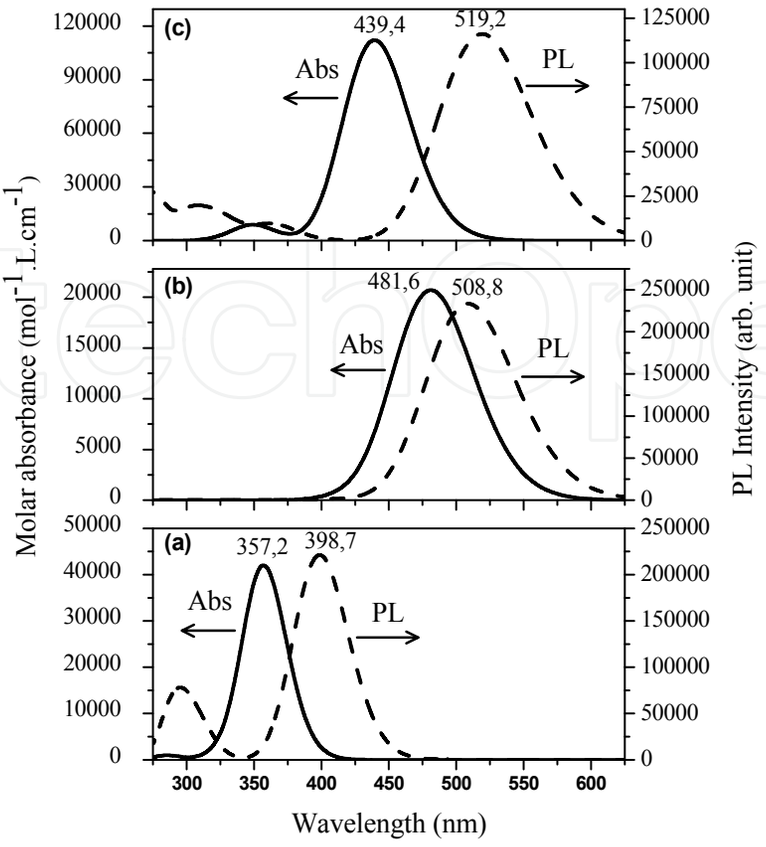

Figure 13. The simulated optical absorption and emission spectra of 2-TBT-BIPY copolymer with CIS/3-21G* (a), TD-B3LYP/3-21G* (b) and ZINDO (c) methods.

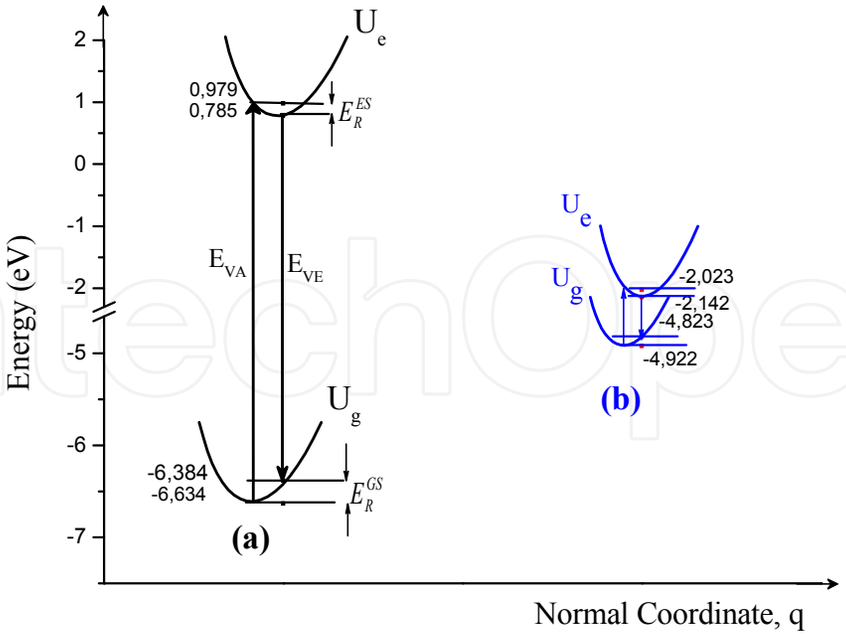

Figure 14. Schematic representation of the potential energy surface (PES) of the ground (U_g) and excited (U_e) states along with their normal mode coordinates of 2-TBT-BIPY copolymer calculated by CIS/3-21G* (a) and TD//B3LYP/3-21G* (b) methods. The parameters indicated are the absorption energy (E_{VA}), emission energy (E_{VE}) and relaxation energy (E_R^{GS}, E_R^{ES}).

For understanding better the results optical absorption and emission spectra calculated by ZINDO method experimental results are presented in Fig. 15. All curves are normalized to unity at their respective maximum. Prior to comparing the results calculated by ZINDO with those of obtained from experiments, it may be noted that no solvent effects have been taken into account in the ZINDO calculation. Keeping this in mind and comparing the spectra shapes, we believe that ZINDO results are in agreement with the experimental ones.

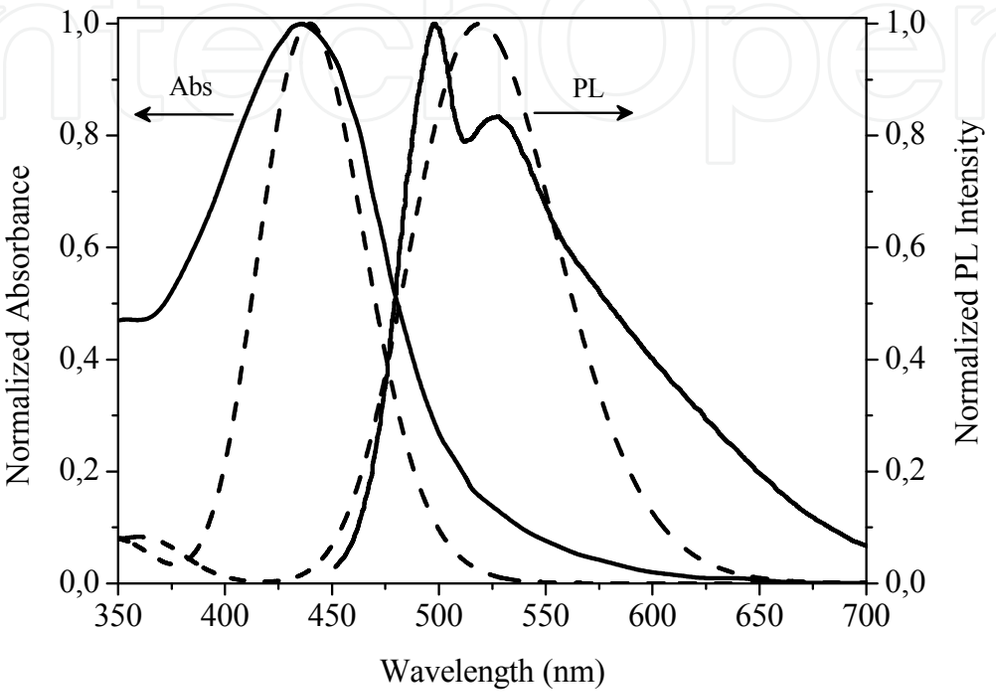

Figure 15. Normalized experimental optical absorption and photoluminescence spectra of TBT-BIPY copolymer (**–**) and those calculated by ZINDO method for 2-TBT-BIPY copolymer (- - -).

3.4. PLEDs architecture

In general, conjugated organic materials have smaller hole injection barriers than electron injection barriers due to the electron richness in a π-conjugated system, leading to poor electron transport ability in these materials. There are two possible approaches to improve this poor electron-transporting ability in organic materials used for fabricating LEDs. The most straightforward modification is to deposit a low work function (WF) metals such as Mg or Ca as cathode by high vacuum sublimation. However, the sensitivity of these metals towards oxygen and moisture limits their practical applications. The other more practical approach is to design or invent a material with lower LUMO energy by increasing its electron affinity, so that LUMO is to WF of the cathode material.

The electron injection energy barrier (ΔE_e) is determined by the electron affinity (EA) or by the difference between LUMO and WF of the cathode (ϕc), while the hole injection energy barrier (ΔE_h) is determined by the difference between IP or HOMO and WF of the anode (ϕa). In the most simple case, a single organic layer OLED, the organic layer is sandwiched between two electrodes of different work functions, one of which has to be transparent to

light. For this electrode ITO coated glass substrates are frequently used. As for the counter electrode aluminum is used mostly.

The energy barriers between the emitting polymer and electrodes can be estimated by comparing the work function of the electrodes with HOMO and LUMO energy levels of emitting polymer. Thus, the hole-injection barrier is $\Delta Eh = E_{HOMO}$-4.8 eV, where 4.8 eV is the work function of the ITO anode and the electron-injection barrier is $\Delta E_e = \phi_X - E_{LUMO}$, where ϕ_X is the work function of cathode. The difference between the electron- and hole-injection barriers (ΔE_e-ΔE_h) is a useful parameter to evaluate the balance in electron and hole injection. Lower the (ΔE_e-ΔE_h) better the injection balance of electrons and holes from the cathode and anode, respectively. For TBT-BIPY copolymer, we have shown in Fig.16 the energy level diagrams of a single-layer PLED.

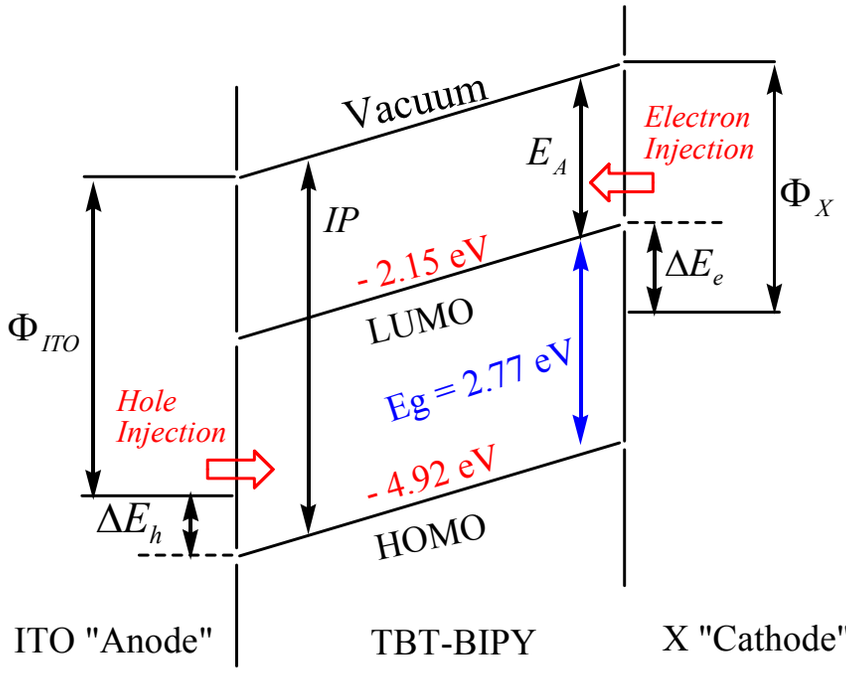

Figure 16. Energy-level diagrams of a single-layer PLED (ITO/TBT-BIPY/AL, Mg or Ca).

The ionization potentials (IP) and electron affinity (EA) are calculated by DFT/B3LYP/3-21G*on the geometry of the neutral, cationic and anionic states to estimate the energy barrier for the injection of both holes and electrons into TBT-BIPY copolymer. The calculated values are obtained as 5.62 eV and 1.35 eV, respectively. From Table 5, we showed that low work function metals such as Mg or Ca are typically used to minimize the barrier and then to provide for an ohmic contact.

X	ϕ_X (eV)	ΔE_h (eV)	ΔE_e (eV)	ΔE_e-ΔE_h (eV)
Al	4.2	0.12	2.05	1.93
Mg	3.6	0.12	1.45	1.33
Ca	2.8	0.12	0.65	0.53

Table 5. Parameters to evaluating the balance in electron and hole injections in PLED.

4. Part II: Donor-acceptor polymers for photovoltaic cell devices

4.1. Results and discussion

4.1.1. Conformational study

As first step, an accurate representation of the bond rotations in the chain is extremely important, since the properties of such polymers depend strongly on the conformational statistics of polymer chains [119]. Besides, the geometries obtained for the most stable conformations are used as input data for full optimization calculations. DFT/B3LYP calculations are performed on the following three model compounds, poly(3-hexylthiophene)-benzothiadiazole (P3HTBT), poly (carbazole-benzothiadiazole) (PCzBT) and poly(3-hexylthiophene)- di-benzothiadiazole-carbazole (P3HT2BTCz).

In conformational part, two basis sets 3-21G* and 6-31G* have been used for the sake of comparison. We note that the results derived from these two basis sets are almost similar. The relative energy for the first model (Fig. 17) shows two local minima in both sides of the spectrum (0° and 180°) and a maximum at about 90°.

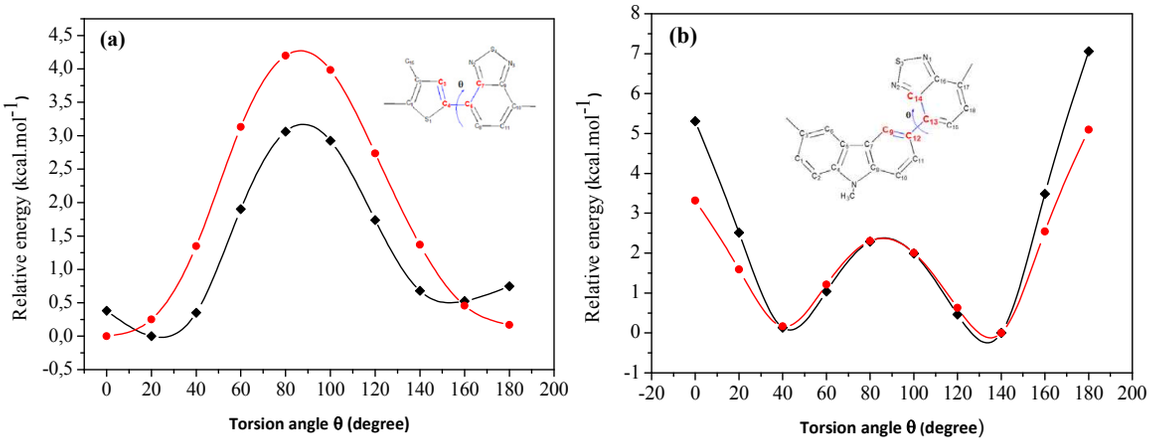

Figure 17. Potential energy curves of: (a) P3HTBT and (b) PCzBT monomer simulated at DFT/B3LYP level with (–•–) 3-21G* and (–♦–) 6-31G* basis sets.

The results indicate that the P3HTBT is completely planar with the inter-ring torsion angle 0°. It's obvious that this planarity is caused by intra-molecular repulsion between sulphur atoms in the main polymer backbone. In the case of benzothiadiazole copolymerized with carbazole, the conformational behaviour is completely different. The twisted conformations have two torsion angles θ_1 and θ_2 at around 40° and 140°, respectively. The latter conformation (140°) is slightly more stable by about 0.5 kcal.mol^{-1}.

4.1.2. Structural and characteristic parameters

The fully optimized structures with DFT/B3LYP/3-21G* method, with the respect to the torsion angles of both P3HTBT and PCzBT copolymers are shown in Fig. 18.

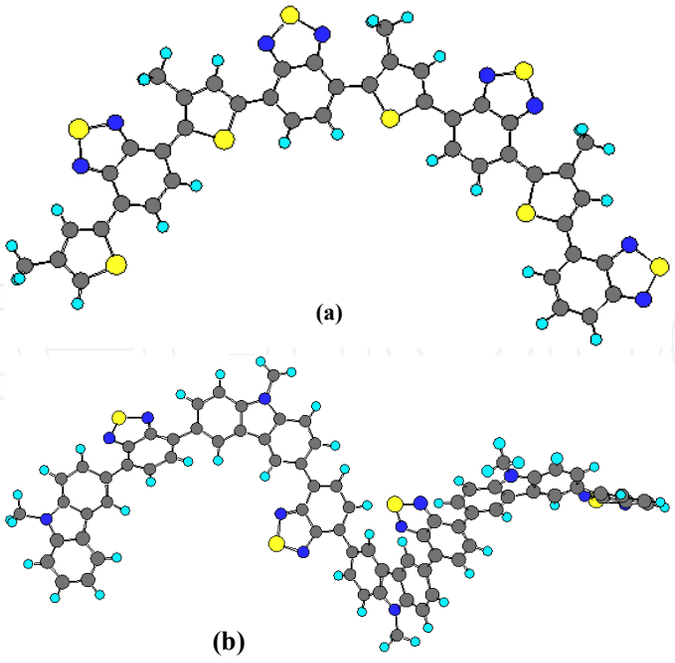

Figure 18. DFT/B3LYP/3-21G* optimized structure of: (a) $(P3HTBT)_4$ copolymer and (b) $(PCzBT)_4$ copolymer.

Based on these optimized structures, the principal physico-chemical parameters of the two copolymers are collected in Table 6. Along with the torsional angle (θ) (the deviation from co-planarity between the donor and acceptor units), intra-molecular charge transfer (D_{CT}) (the summation of all charges for the donor unit 3-hexyl thiophene (3HT) and carbazole (Cz)), bridge length (L_B) (the bond length between the donor and acceptor) are summarized.

	L_B (Å)	D_{CT} (e)	θ (°)
P3HTBT	1.458	0.038	0.0
PCzBT	1.482	0.063	147.0

Table 6. The optimum characteristic parameters (L_B, D_{CT}, and θ) of P3HTBT and PCzBT model compounds.

Considering the most stable conformation, we can deduce that the optimized structure of the PCzBT appears under a twisted configuration with a large torsional angle (θ = 147.0°). This suggests that a strong steric hindrance effect exists between the donor and acceptor moieties, whereas the P3HTBT structure has perfectly a planar structure. Moreover, compared to PCzBT, the order of the L_B of P3HTBT remains smaller indicating the formation of the mesomeric structures induced by intra-molecular charge transfer, that is, D-A→←D^+=A^-. The large intra-molecular charge (D_{CT}) of PCzBT copolymer backbone is probably originating from the nitrogen atoms with high electronegativity in the main backbone of Cz donor group. DCT significantly enhances the π-electron delocalization which is largely dependent on θ rather than on the acceptor strength.

The optimized structure of the resulting P3HT2BTCz composite and its main geometrical parameters (torsion angle and interring bond length) are illustrated in Fig. 19. The inspection of these data reveals that the resulting composite shows an almost non planar conformation which is more underlined on both sides of carbazole units to reach the values of 45° and 49°. Moreover, compared to those of P3HTBT and PCzBT, the central bonds connecting the two neighbouring central rings are slightly shorter, showing that this compound is more conjugated to extend the delocalization on all the chain backbone.

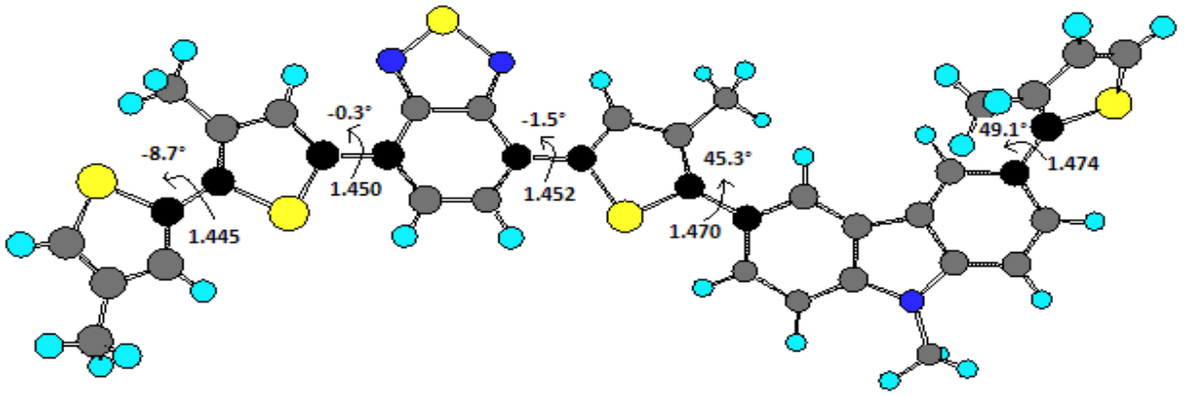

Figure 19. DFT/B3LYP/3-21G* optimized geometric structure of the resulting P3HT2BTCz composite.

4.1.3. Optical properties and electronic structures

As firstly discussed, the oligomer geometries and their corresponding band gap are calculated using DFT/B3LYP method with 3-21G* and 6-31G* basis sets. The band gap is estimated as the difference between the HOMO and LUMO energies. In our case, the band gap of $(P3HTBT)_n$ and $(PCzBT)_n$ (n = 1-4) oligomers are listed in Table 7.

Polymer	Number of monomer	Band gap energy (E_g) (eV)	
		B3LYP/3-21G*	B3LYP/6-31G*
P3HTBT	1	3.23	3.26
	2	2.67	2.45
	3	2.11	2.12
	4	1.94	1.96
	∞	1.61	1.55
PCzBT	1	3.10	3.09
	2	2.80	2.82
	3	2.71	2.63
	4	2.68	2.61
	∞	2.52	2.44

Table 7. Band gap energy E_g of $(P3HTBT)_n$ and $(PCzBT)_n$ (n: from 1 to 4 units).

By using the linear extrapolation technique [120], it can be seen from Fig. 20 that this value decreases with increasing the chain length from monomer to quatermer. Moreover, the theoretical data resulting from the two considered basis sets are very close and no significant changes are noticed when going from 3-21G* to 6-31G* basis set calculations.

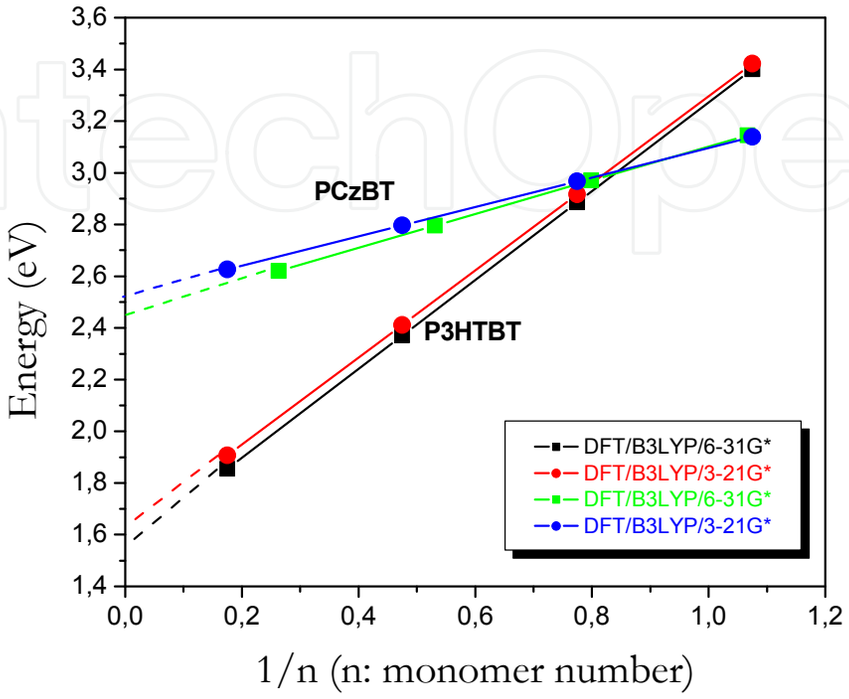

Figure 20. Representation of the band gap energy (E_g) as function of inverse chain length (1/n) for P3HTBT and PCzBT calculated by DFT/B3LYP with 6-31G* and 3-21G*basis sets.

The band gap of P3HTBT is found to be around 1.55 and 1.61 eV with 6-31G* and 3-21G* basis sets, respectively. These values are lower than that of pristine P3HT (1.90 eV) [121], due to the presence of benzothiadiazole in the main backbone copolymer. In parallel, a wide band gap for PCzBT is estimated to be 2.44-2.52 eV (Fig. 20). Nevertheless, the band gap of resulting composite P3HT2BTCz is found to be 2.31 eV which is in agreement with the experimental values $E_g \approx 1.97$ eV (derived from the UV-visible absorption spectrum in chloroform solution) [87]. These results are in close agreement with the experimental data by taking into account the packing effects (interchain interaction) in the solid state [122]. The HOMO level energy is estimated to be - 4.9 eV making this copolymer photo-chemically stable.

The TDDFT method was applied on the basis of the ground state optimized geometry of different compounds under study. As shown in Fig. 21, the absorption spectrum of the P3HT2BTCz composite seems to be the superposition of the two absorption spectra of P3HTBT and PCzBT copolymers. Compared to PCzBT and P3HTBT polymers, the absorption spectra is broader due the red shifted absorption, which may be attributed to the much better conjugation along the polymer backbone. Besides, the simulated absorption spectra show that the P3HT2BTCz compound absorbs from the UV at a wavelength of 600 nm, with two main absorption peaks centred at 478 and 319 and a weak peak at 260 nm. The

band located at 319 nm arises from the delocalized π→π* transition in the polymer and the visible absorption peak located at longer wavelength centered at 478 nm could be assigned to the intra-molecular charge transfer transition between the Cz donor moiety and the BT acceptor unit [123].

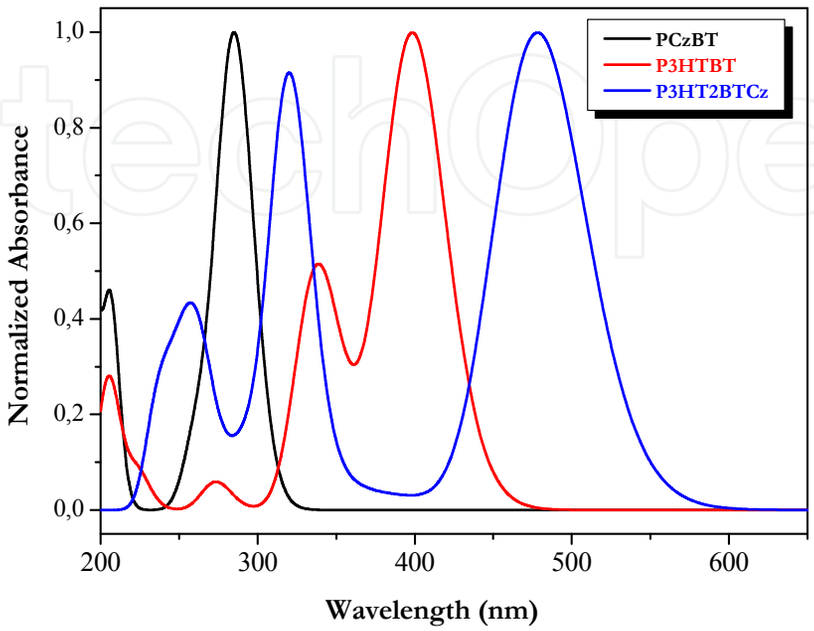

Figure 21. TD/B3LYP/3-21G* simulated UV-Visible optical absorption spectra: of PCzBT, P3HTBT and P3HT2BTCz.

The vertical excitation energy and their corresponding oscillator strength along the main excitation configuration are listed in Table 8. The first optically allowed electronic transition of P3HT2BTCz populates the HOMO→LUMO excitation with high oscillator strength (f = 1.0898). The two other transitions are mainly assigned respectively to HOMO→LUMO+1 and HOMO-1→LUMO+3 excitations. All intermediate states with low oscillator strength, so-called dark states, have intra-molecular charge transfer (ICT) character. Through this study, it is found that the calculated results reproduce very well the corresponding experimental data [87].

Electronic transition	Wavelength (nm)	Oscillator Strength (f)	Main MO/character	Coefficient	Experimental value (nm)
$S_0 \rightarrow S_1$	478	1.0898	HOMO→LUMO	80%	504[a] 518[b]
$S_0 \rightarrow S_2$	319	0.6912	HOMO→LUMO+1	51%	327[a] 338[b]
$S_0 \rightarrow S_3$	260	0.1905	HOMO-1→LUMO+3	54%	----

[a]in chloroform solution [87]
[b]in solid film [87]

Table 8. Main electronic transitions in P3HT2BTCz composites and their assignments.

In order to study the emission properties of P3HT2BTCz compounds, the TD/B3LYP method was applied to the geometry of the lowest singlet excited state optimized at the CIS level with 3-21G* basis set [124]. The normalized photoluminescence (PL) spectrum of P3HT2BTCz (Fig. 22) shows a maximum at 649 nm with strongest intensity (f = 0.8415), compared to 630 nm in experimental spectrum as indicated in Table 9. This may be regarded as an electronic transition reverse of the absorption corresponding mainly from LUMO to HOMO. Moreover, the observed red-shifted emission in the PL spectra is found to be in reasonable agreement with the experimental one by taking into account the packing effects (inter-chain interaction) in the solid state (0.49 eV (124 nm)) [87].

Electronic transition	Emission wavelength (nm)	Emission energy (cm^{-1})	Oscillator Strength (f)	MO/character	Coefficient	Experimental value (nm)
$S_1 \rightarrow S_0$	649	15400	0.8415	HOMO→LUMO	75%	630[a]

[a]in chloroform solution [87]

Table 9. Emission energy of P3HT2BTCz obtained by the TDDFT/B3LYP/3-21G* method.

We also find relatively high values of Stokes Shift (SS) in P3HT2BTCz (0.62 eV (172 nm)) (Fig. 22).

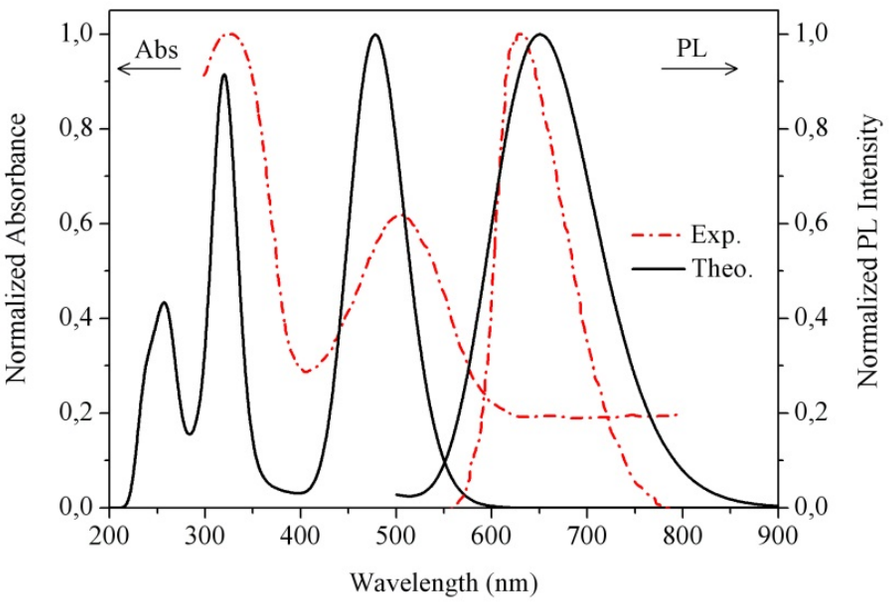

Figure 22. Experimental and TD-DFT calculated normalized absorption and emission spectra of P3HT2BTCz.

Based on the above results, the energy band structures are plotted in Fig. 23. When carbazole (Cz) is replaced by 3-hexylthiophene (3HT), the energy of HOMO level increases,

while that of LUMO decreases. This change on the electronic structure facilitates both the hole and electron-transporting ability. The electronic structure differs greatly from one model to another, showing the effect of donor units in D-A architecture polymer and it results from the coupling behaviour of 3HT, Cz and BT in the main backbone. Moreover, further insights are obtained comparing the DFT calculated density of states (DOS) of the P3HTBT and PCzBT with that of P3HT2BTCz composite. This comparison is showed in Fig. 23 (at the right). Two striking things immerge from DOS diagram: 1) the ground state interaction between the donor and acceptor units and 2) this interaction induces intra-gap charge transfer states lying inside the gap of the PCzBT. As a result, P3HT2BTCz composite orbitals are shifted towards higher energies compared to the isolated PCzBT orbitals and towards lower energies compared to the isolated P3HTBT orbitals.

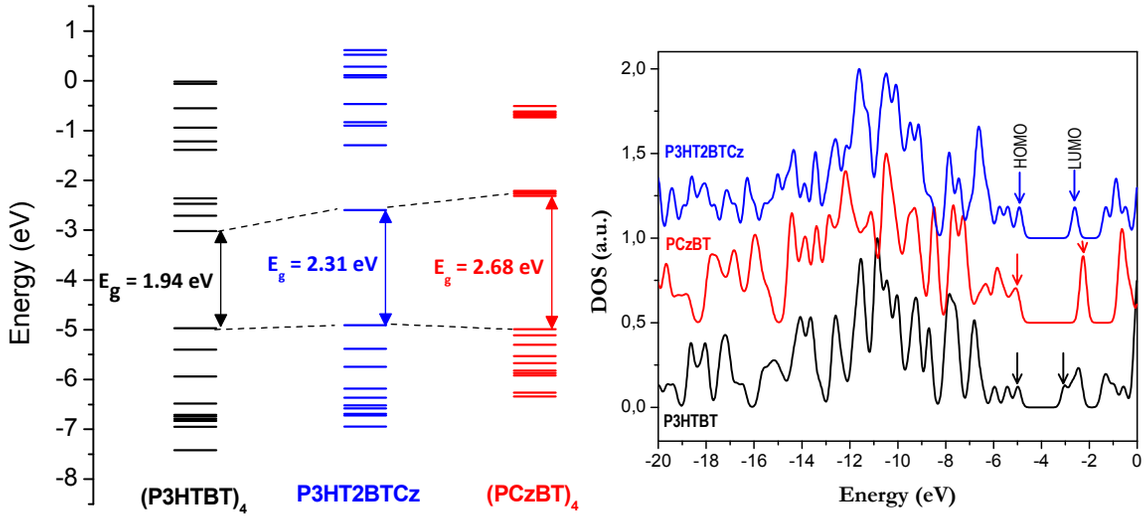

Figure 23. Electronic structure and DOS diagram of P3HTBT, PCzBT and P3HT2BTCz, simulated using DFT/B3LYP/3-21G* method.

The electron density iso-contours of HOMO and LUMO of P3HT2BTCz compound are plotted in Fig. 24. It can be seen that an asymmetric character within the rings and between subunits prevails for the HOMO orbital of this copolymer. Moreover, the localization of electronic charge lies mainly in the side part of HOMO orbital, which is typically expected due to the chain-end effects, which changes the shape of LUMO orbital. Due to the non-planarity observed for the P3HT2BTCz compound geometry, in its ground state, electrons are mainly localized on the benzothiadiazole units, as result of the weak interactions between the two building blocks. This fact is particularly noticeable in the LUMO orbital with a symmetric character between the subunits.

According to our calculations, electron densities in the first excited state namely LUMO and LUMO+1 are delocalized on BT and P3HT units with a symmetric character. Whereas, for higher energy levels, e.g., LUMO+2 levels take part in electron transitions on the P3HT and Cz units. Yet, the charge density of HOMO, HOMO-1 shows that the charge density spreads over the main chain of the compound to become much concentrated around the P3HT and Cz units in HOMO-2.

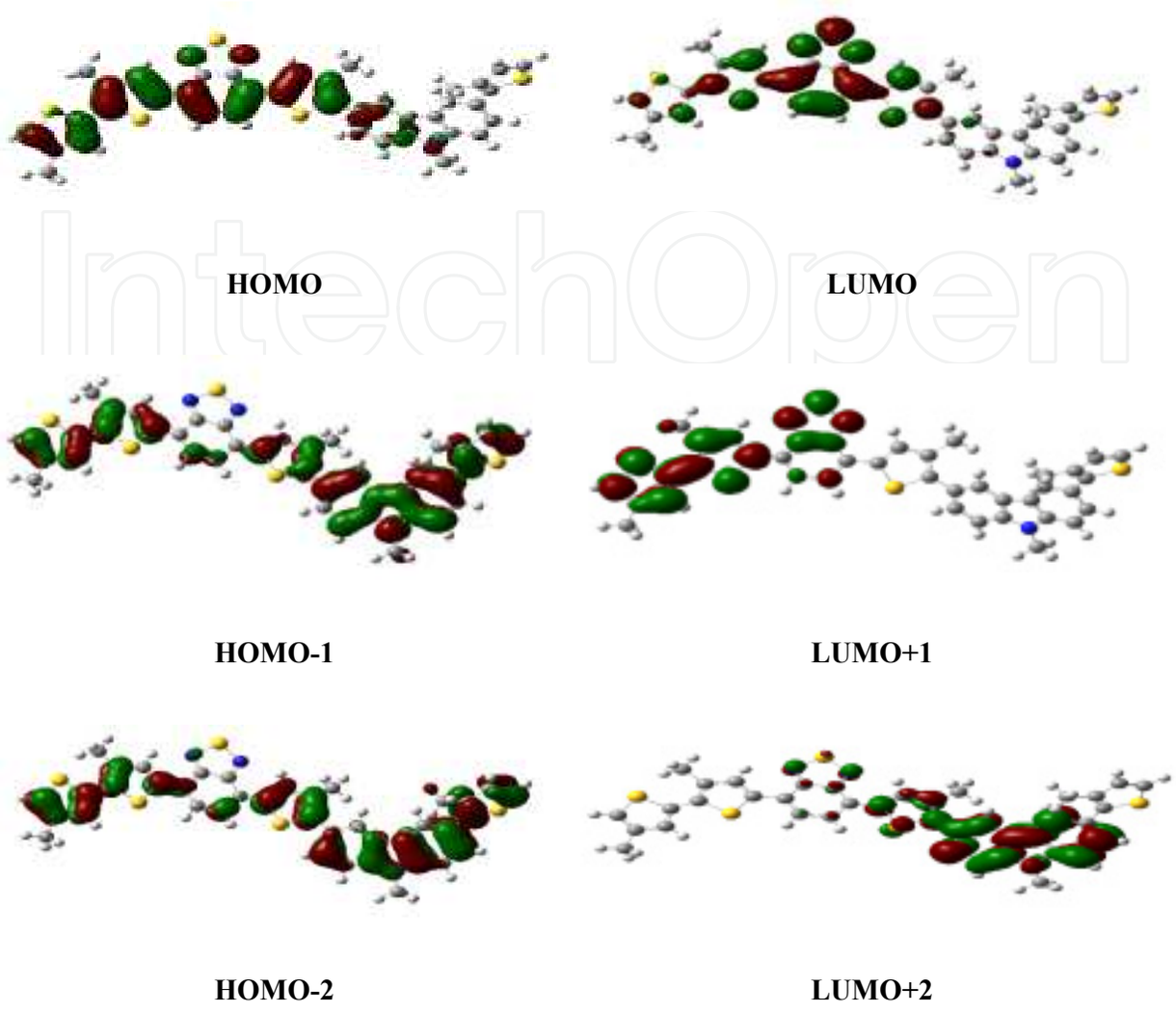

Figure 24. Contour plots for the main HOMO and LUMO molecular orbitals of P3HT2BTCz compound.

4.1.4. Vibrational study and force constant analysis

The most intense calculated bands of the infrared absorption (IR) of these compounds, shown in Fig. 25 are collected in Table 10 together with their corresponding assignments.

PBT		P3HTBT		PCzBT		P3HT2BTCz		Assignments
υ (cm^{-1})	I	υ (cm^{-1})	I	υ (cm^{-1})	I	υ (cm^{-1})	I	
707	m	725	w	728	w	-	-	Out of plan C-H wagging (BT + Cz).
-	-	957	w	-	-	-	-	Ring breathing (BT and P3HT).
956	s	961	w	960	vw	947	vw	S-N Scissoring (BT).
1080	s	1024	s	1037	w	1037	vw	S-N stretching (BT) + Rocking CH_3 (P3HT and Cz).

1234	vw	1234	w	1231	w	1224	w	C-H Rocking (3HT + Cz) + C-H wagging (BT)
-	-	1350	w	-	-	1347	w	CH_3 Wagging (3HT).
-	-	-	-	1372	w	1372	-	CH_3 Scissoring (Cz).
		-	-	1432	w	1429	w	C=C stretching (Cz).
1445	s	1445	vw	-	-	-	-	Ring vibration.
1514	vw	1516	m	-	-	1516	m	Ring vibration + C-H Rocking.
-	-	-	-	1582	m	-	-	Aromatic C-H and C-C stretching (Cz and BT).
-	-	1607	m	-	-	-	-	C=C ring stretch (P3HT and BT).
1621	w	-	-	-	-	-	-	C-C Bending vibration (BT).
-	-	-	-	1646	m	1652	s	C=C bending (Cz).
-	-	1675	w	-	-	1652	s	Antisymmetric C=C stretching (3HT).
-	-	1690	w	-	-	1689	w	Symmetric C=C stretching (3HT).
1792	m	1787	m	-	-	-	-	C-C Bending (BT).
		-	-	1792	s	1791	s	Symmetric C-C stretching (Cz).
-	-	-	-	1841	m	1841	w	C-N Scissoring and C-C stretching (Cz).
3330	vs	3310	S	3312	s	-	-	C-H stretching (BT).

Table 10. Main selected infrared modes of PBT, P3HTBT, PCzBT and P3HT2BTCz and their corresponding assignments (υ: frequency, I: intensity, s: strong, vs: very strong, m: medium, w: weak, vw: very weak).

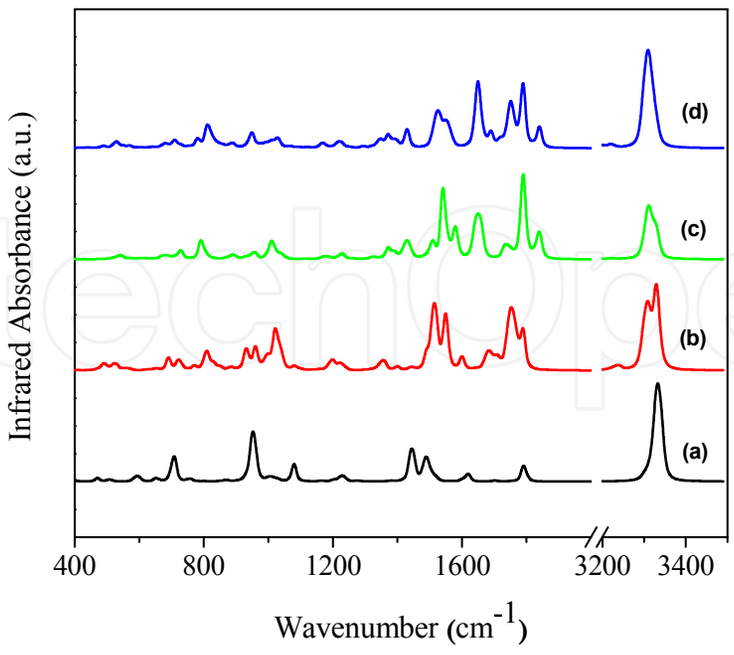

Figure 25. Theoretical infrared spectra of: (a) PBT, (b) P3HTBT, (c) PCzBT and (d) P3HT2BTCz.

A large number of bands appear with very high peaks due to an induced strong dipolar moment. All characteristics of infrared bands in P3HT [125], PCz and BT vibration modes are observed.

The inspection of these spectra shows that after combining the two copolymers to obtain the P3HT2BTCz composite, some bands undergo slight changes in their positions and intensities. The main vibrational modes of PBT persist following the addition of 3HT, Cz groups in the P3HT2BTCz composite. Firstly, a down shift of the band assigned to C-H stretching in benzothiadiazole unit is observed at high frequencies with strong intensity located at 3330 cm^{-1} in $(P3HTBT)_4$ and $(PCzBT)_4$.. The band at 1785 cm^{-1} assigned to the anti-symmetric C=C stretching mode becomes clear in the other PCzBT and P3HT2BTCz compounds and the C-C bending vibrational mode located at 1621 cm^{-1} in PBT becomes clearly pronounced in PCzBT and P3HT2BTCz with a high energy shift of about 20 cm^{-1}.

The signal attributed to the S-N stretching at 1073 cm^{-1} completely disappears in the functionalized composite following a significant interaction of different groups. This effect is also confirmed by the shift (from 1486 to 1550 cm^{-1} and from 1443 to 1513 cm^{-1}) observed in IR bands ascribed to symmetric and anti-symmetric C=C stretching, respectively, as a consequence of the presence of more conjugated backbone. The band at 707 cm^{-1}, ascribed as out-of-plane C-H wagging of PBT polymer, decreases in intensity in the first two copolymers and disappears completely in the case of the P3HT2BTCz composite. This effect is due to a significant interaction between donor Cz as donor and BT as acceptor acceptor groups. Thus, this analysis highlights the effective charge transfer in the main backbone of these compounds targeted for photovoltaic applications.

In order to support the above discussed results further, the force constant analysis of benzothiadiazole unit in P3HTBT, PCzBT copolymers and P3HT2BTCz composite, have been investigated as shown in Fig. 26.

Generally, the bond stretch depends on two main parameters, the bonding energy (E_0) and the force constant k. The latter represents the potential energy surface (PES) curvature near the minimum $k = (\frac{\partial^2 E}{\partial R^2})_{R=R_0}$. The force constant (k) is proportional to the strength of the covalent bond [126]. Considering the BT unit as shown in Fig. 26, one can deduce that the bond length variation marks important changes in benzothiadiazole bonding, depending on the electronic configuration and hence force constant. One can also notice that the inter-ring force constants (F_1 and F_{12}) increase dramatically with a significant decrease in their corresponding bond length, leading to a more conjugated composite compared to P3HTBT and PCzBT. It clearly shows that the intra-ring delocalization is larger for P3HT2BTCz than for P3HTBT or PCzBT. In addition, the modifications on benzene moiety are clearly seen through the force constants F_5 and F_7. On the thiadiazole part, force constants such as F_8, F_9, F_{10} and F_{11} are very similar but a slight variation can be noticed in the case of the composite because of the presence of Cz and BT together in the main backbone structure with 3HT as spacer. This configuration can enhance the charge transfer between donor and acceptor units. These observations are consistent with the above discussed properties.

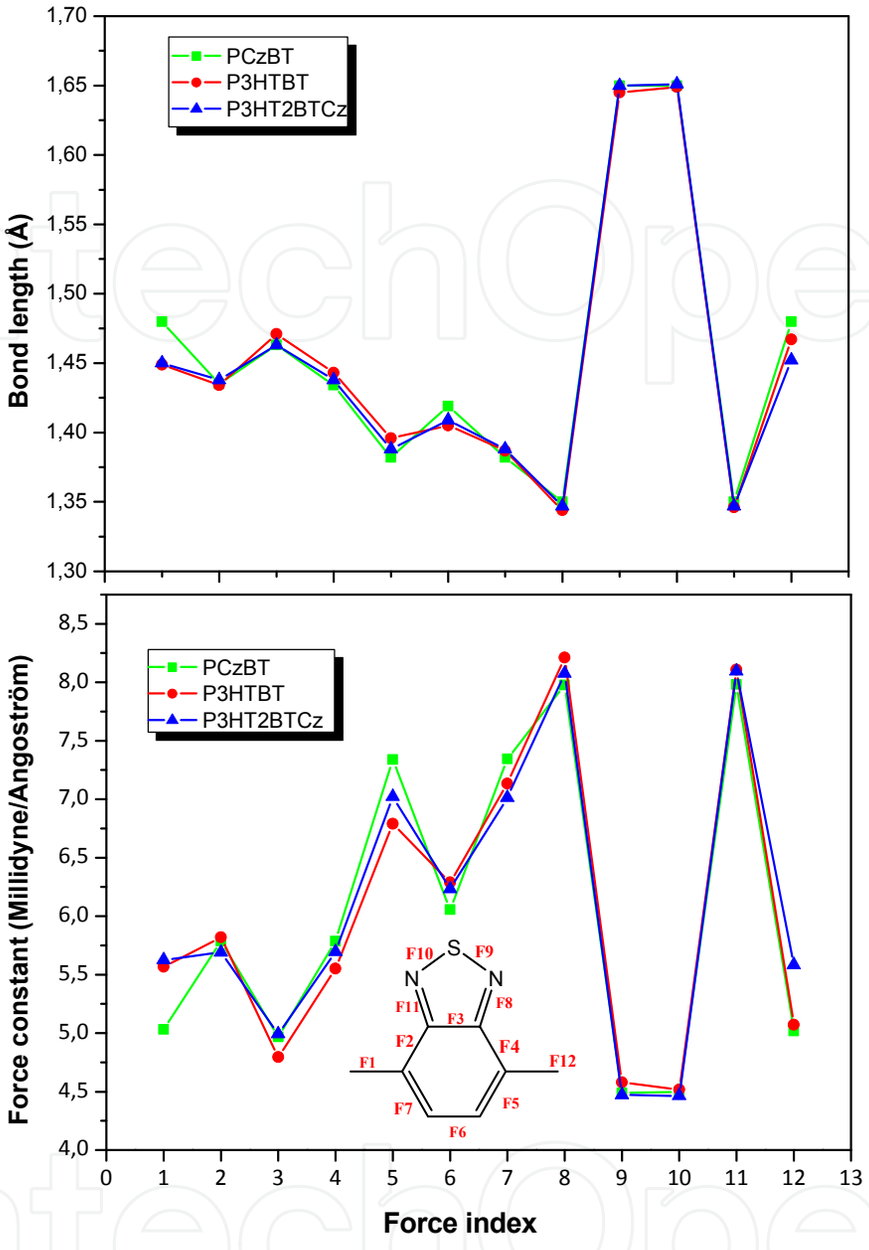

Figure 26. Main force constants and bond lengths of equivalents benzothiadiazole sites.

4.2. Photovoltaic properties

Favorable values of HOMO and LUMO levels, band gaps, and strong absorptions in the visible region suggest that the P3HT2BTCz may be used as active layer in PSCs devices when blended with [6,6]-phenyl-C_{61}-butyric acid methyl ester (PCBM), which is the most broadly used acceptor in solar cell devices [127-128]. After an optimization procedure via the semi-empirical PM3 method, the resulting blend geometrical structure of the composite (P3HT2BTCz:PCBM) in weight ratio of 1:1 is then re-optimized by DFT/B3LYP/3-21G* as

shown in Fig. 27, where the substituents in the case of PCBM play the role of the spacers between the donor and C_{60} acceptor units. This stable configuration is governed by the interaction of oxygen of the PCBM with the sulphur atom of thiophene units on both sides of carbazole motives.

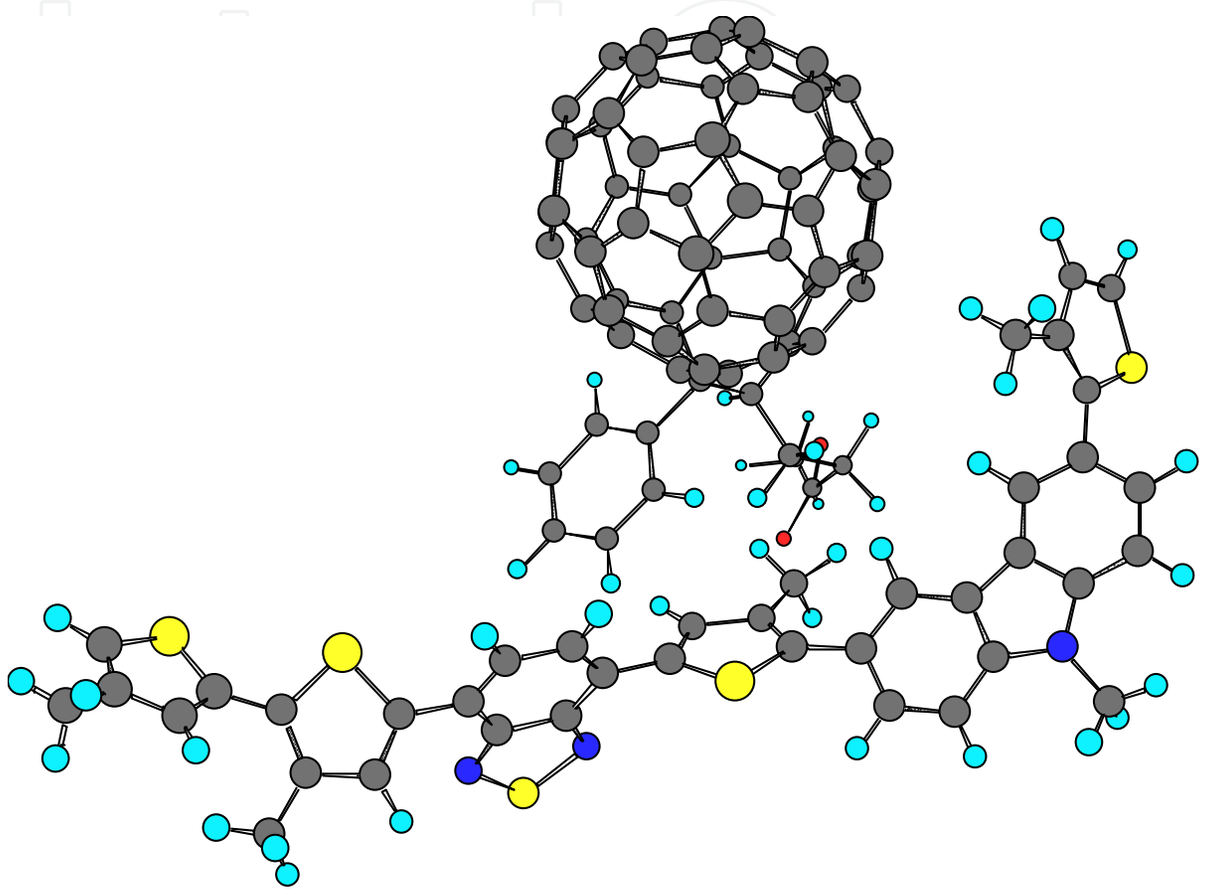

Figure 27. Optimized geometric structure of P3HT2BTCz:PCBM (1:1) simulated by DFT/B3LYP/3-21G* method.

Based on the comparison between the donor and the acceptor compounds, the resulting composite shows some interesting electronic properties, such as a low band gap of 1.93 eV and a lower HOMO energy level of -5.32 eV which indicate that this composite can be used as an active layer in photovoltaic cells. The corresponding structure of a photovoltaic device is schematically presented in Fig. 27. The difference in the LUMO energy levels of P3HT2BTCz and PCBM is close to 1.0 eV, suggesting that the photo-excited electron transfer from P3HT2BTCz to PCBM may be sufficiently efficient in photovoltaic devices [129-130]. Energetically, in comparing different anode and cathode metals as shown in Fig. 28 one can notice that the transparent ITO (Indium Tin Oxide) anode and Al, Ag or Mg (Aluminium, Silver or Magnesium) as cathode are the most suitable metals for for effective charge collection on two electrodes.

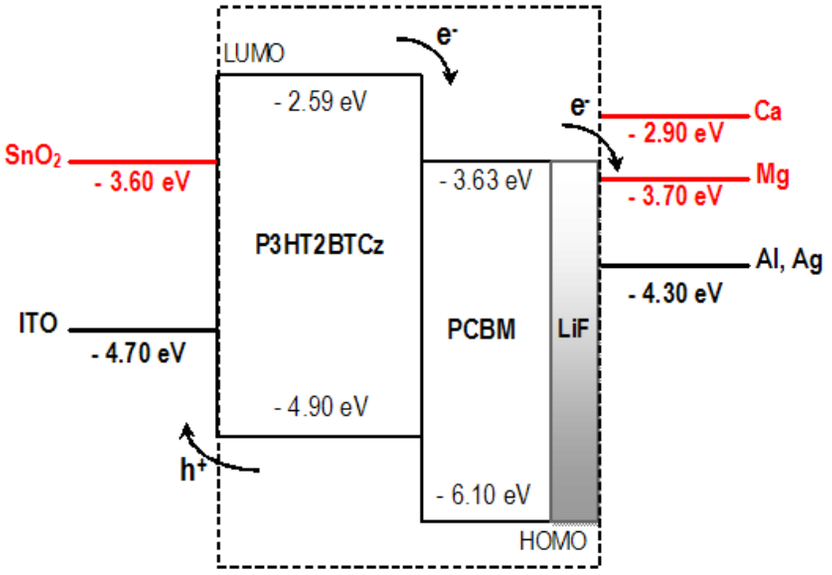

Figure 28. Schematic energy diagram of the proposed bulk heterojunction solar cell.

The photovoltaic efficiency performance data of the photovoltaic cell (power conversion efficiency (PCE) values, including the open circuit voltage (V_{oc}), short circuit current (J_{sc}), fill factor (FF) and incident-light power (Pin), are derived from the following equation: PCE = V_{oc}. J_{sc}. FF/P_{in}. The maximum open circuit voltage (V_{oc}) of the BHJ solar cell is related to the difference between HOMO of the electron donor and LUMO of the electron acceptor, taking into account the energy lost during the photo-charge generation [131-133]. The theoretical values of open-circuit voltage V_{oc} have been calculated from the following expression [134]:

$$V_{OC} = |E(HOMO)^{donor}| - |E(LUMO)^{acceptor}| - 0.3$$

Based on this formula, it can be seen that the V_{oc} value of P3HT2BTCz: PCBM is about 0.97 V but it depends on the difference of the output of the electrodes [135]. Starting from the above results, P3HT2BTCz composite seems to be a good candidate for photovoltaic application due to its high V_{oc} and wider absorption range broader than the range of absorption of other copolymers. Based on Scharber model [136], the maximum power-conversion efficiency of the photovoltaic solar cell, with P3HT2BTCz:$PC_{61}BM$ (1:1) composite as active layer can be up to 5%.

5. Conclusion

The aim of this chapter is to combine experimental analyses and theoretical calculations to present a comprehensive study of the structural and optical properties of organic electronic devices. Based on model compounds, Highest Occupied Molecular Orbital (HOMO), Lowest Unoccupied Molecular Orbital (LUMO) levels, Ionization Potential (IP), Electron Affinity (EA) as well as electronic structures for two samples are examined. The optoelectronic parameters studied here are essential for better understanding of the exchange between polymer and electrodes in PLEDs and PPCs. The experimental and computational results are compared and discussed.

The first part of this chapter shows how important it is to combine thienylene, dialkoxyphenylene and bipyridine fragments to obtain compounds with a strong electronic delocalization. As a result, analysis of the results obtained in the gas phase has allowed us to understand the crucial role played by the intra-molecular S--O and N--H interactions in determining the planarity of the compound. This leads to the formation of a donor–acceptor type of arrangement within the polymer backbone and an intra-molecular charge transfer for the TBT-BIPY copolymer model compound. In addition, we have presented the optical and emission properties of these compounds by studying the ground and first excited states of copolymer models.

In the second part, we have used the density functional theory DFT/B3LYP to investigate the photo-physical properties of some copolymers in alternate donor-acceptor structure. In fact, the modification of chemical structures can greatly modulate and improve the electronic and optical properties of pristine copolymers. Hence, added to benzothiadiazole units, the introduction of carbazole motives in the copolymer backbone results in a better overlap of the absorption spectrum with the solar spectrum. In addition, the hexylthiophene linkage is found not only as a conjugated bridge but also it reduces the steric interaction between aromatic rings and thus enhances the effective charge transfer between donor and acceptor units.

In fact, the obtained theoretical data derived from DFT/B3LYP/3-21G* method are in good agreement with the available experimental data. The resulting optimized BHJ active layer shows a π-stacking configuration governed by a Wander walls interaction. A model energy band diagram is introduced, simulating the energy behaviour of this active layer. Based on this design concept, the PSC using the blend of P3HT2BTCz with fullerene derivatives, exhibit a promising performance with a PCE up to 5%. This approach provides great flexibility in fine-tuning of the absorption spectra and energy levels of the resultant polymers for achieving high device performance.

Finally, these results clearly indicate that these new compounds with alternating donor-acceptor structures are promising materials for application in optoelectronic devices. Devices fabrication and characterization are in progress and will be published elsewhere.

Author details

S. Ayachi, A. Mabrouk and K. Alimi*
Research Unit: New Materials and Organic Electronic Devices (UR 11ES55), Faculty of Sciences of Monastir, University of Monastir, Tunisia

M. Bouachrine
UMIM, Polydisciplinary Faculty of Taza, University Sidi Mohamed Ben Abdellah, Taza, Morocco

Acknowledgement

This work has been supported by the cooperation Tunisio-Marocain (CMPTM No. 11/TM/72) and Tunisian-French cooperative action (CMCU/07G1309).

* Corresponding Author

6. References

[1] Chiang C.K, Fincher C.R. Jr, Park Y.W, Heeger A.J, Shirakawa H, Louis E.J, Gau S.C, MacDiarmid, A.G, Phys. Rev. Lett. 39, 1098 (1977).

[2] Chiang C.K, Druy M.A, Gau S.C, Heeger A.J, Louis E.J, MacDiarmid A.G, Park Y.W, Shirakawa H, J. Am. Chem. Soc., 100, 1013 (1978).

[3] Balan A, Baran D, Gunbas G, Durmus A, Ozyurt F, Toppare L, Chem. Commun. 44, 6768 (2009).

[4] Thompson, B.C, Kim, Y-G, McCarley T.D, Reynolds J.R, J. Am. Chem. Soc. 128, 12714 (2006).

[5] Kraft A, Grimsdale AC, Holmes A.B, Ange. Chem. Intern. Ed. 37, 402 (1998).

[6] Evans N.R, Devi L.S, Mak C.S.K, Watkins, S.E, Pascu S.I, Kohler A, Friend R.H, Williams C.K, Holmes A.B, J. Am. Chem. Soc., 128, 6647 (2006). Huang Q, Evmenenko G.A, Dutta P, Lee P, Armstrong N.R, Marks T.J, J. Am. Chem. Soc. 127, 10227 (2005).

[8] Tsuji H, Mitsui C, Sato Y, Nakamura E, Adv. Mater. 21, 3776 (2009).

[9] Zhen C.G, Chen Z.K, Liu. Q.D, Dai Y.F, Shin R.Y.C, Chang, S-Y, Kieffer J, Adv. Mater. 21, 2425 (2009).

[10] Huang J, Qiao X, Xia Y, Zhu X, Ma D, Cao Y, Roncali J, Adv. Mater. 20, 4172 (2008).

[11] Song M.H, Kabra D, Wenger B, Friend R.H, Snaith H, J. Adv. Funct. Mater. 19, 2130 (2009).

[12] Huang F, Chen K.S, Yip H.L, Hau S.K, Acton O, Zhang Y, Luo J, Jen A.K.Y, J. Am. Chem. Soc.131, 13886 (2009).

[13] Bijleveld J.C, Zoombelt A.P, Mathijssen S.G.J, Wienk M.M, Turbiez M, de Leeuw, D.M, Janssen R.A, J. Am. Chem. Soc. 131, 16616 (2009).

[14] Westenhoff S, Howard I.A, Hodgkiss J.M, Kirov K.R, Bronstein H.A, Williams C.K, Greenham N.C, Friend R.H, J. Am. Chem. Soc. 130, 13653 (2008).

[15] Beek W.J.E, Sloof L.H, Wienk M.M, Kroon J.M, Janssen R.A.J, Adv. Funct. Mater. 15, 1703 (2005).

[16] Coakley K.M, McGehee M.D, Chem. Mater. 16, 4533 (2004).

[17] Hoppe H, Sariciftci N.S, J. Mater. Res. 19, 1924 (2004).

[18] Brabec C.J, Sariciftci N.S, Hummelen J.C, Adv. Funct. Mater. 11, 15 (2001).

[19] Günes, S, Baran D, Günbas G, Özyurt F, Fuchsbauer A, Sariciftci N.S, Toppare L, Sol. Energy Mater. Sol. Cells. 92, 1162 (2008).

[20] Zoombelt A.P, Fonrodona M, Wienk M.M, Sieval A.B, Hummelen J.C, Janssen R.A, Org Lett. 11, 903 (2009).

[21] Colladet K, Fourier S, Cleij T.J, Lutsen L, Gelan J, Vanderzande D, Nguyen L.H, Neugebauer H, Sariciftci S, Aguirre A, Janssen G, Goovaerts E, Macromol. 40, 65 (2007).

[22] Sang G, Zhou E, Huang Y, Zou Y, Zhao G, Li Y, J. Phys. Chem. C.113, 5879 (2009).

[23] Friend R.H. Gymer R.W, Holmes A.B, Buffoughes J.H, Marks R.N, Taliani C, Bradley D.D.C, dos Santos D.A, Bradas J.L, Logdlund M, Salaneck W.R, Nature. 397, 121 (1999).

[24] Fong H.H, Pozdin V.A, Amassian A, Malliaras G.G, Smilgies D.M, He M, Gasper S, Zhang F, Sorensen M, J. Am. Chem. Soc. 130, 13202 (2008).

[25] Lin C-J, Lee W-Y, Lu C, Lin H-W, Chen W-C, Macromol. 44, 9565 (2011).

[26] Beaujuge, P.M, Pisula W, Tsao H.N, Ellinger S, Mullen K, Reynolds J.R, J. Am. Chem. Soc. 131, 7514 (2009).

[27] Pang S, Tsao H.N, Feng X, Mullen K, Adv. Mater. 21, 3488 (2009).
[28] Cho S, Lee K, Heeger A.J, Adv. Mater. 21, 1941 (2009).
[29] Gao P, Beckmann D, Tsao H.N, Feng X, Enkelmann V, Baumgarten M, Pisula W, Müllen K, Adv. Mater. 21, 213 (2009).
[30] McCulloch I, Heeney M, Bailey C, Genevicius K, MacDonald I, Shkunov M, Sparrowe D, Tierney S, Wagner R, Zhang W, Chabinyc M.L, Kline R.J, McGehee M.D, Toney M.F, Nat. Mater. 5, 328 (2006).
[31] Chua L.L, Zaumseil J, Chang J.F, Ou E.C.W, Ho P.K.H, Sirringhaus H, Friend R.H, Nature. 434, 194 (2005).
[32] Irringhaus H, Brown P.J, Friend R.H, Nielsen M.M, Bechgaard K, Langeveld B.M.W, Spiering A.J.H, Janssen R.A.J, Meijer E.W, Herwig P, de Leeuw D.M, Nature. 401, 685 (1999).
[33] Horowitz, G, Adv. Mater. 10, 365 (1998).
[34] Burroughes J.H, Bradley D.D.C, Brown A.R, Marks R.N, Mackay K, Friend R.H, Bum P.L, Holmes A.B, Nature. 347, 539 (1990).
[35] Lin Y-J, Chou W-Y, Lin S-T, Appl. Phys. Lett. 88, 071108 (2006).
[36] Curtis M.D, Macromol. 34, 7905 (2001).
[37] Lee D.W, Kwon K.Y, Jin J.I, Park Y, Kim Y.R, Wang I.W, Chem. Mater. 13, 565 (2001).
[38] Benincori T, Consinni V, Gramatica P, Pilati T, Rizzo S, Sannicolo F, Odeschini R.T, Zotti G, Chem. Mater. 13, 665 (2001).
[39] Yang Y, Pei Q, Heeger A.J, Synth. Met. 78, 263 (1996).
[40] Grem. G, Leditzky. G, Leising. G, Adv. Mater. 4, 36 (1992).
[41] Grem. G, Leising. G, Synth. Met. 57, 4105 (1993).
[42] Berggren M, Inganas O, Gustafsson G, Rasmusson J, Anderson M.R, Hjertberg T, Wennerström O, Nature. 372, 444 (1994).
[43] Pei J, Yu W-L, Ni J, Lai L-H, Huang W, Heeger A.J, Macromol. 34, 7241 (2001).
[44] Pei Q, Yang Y, J. Am. Chem. Soc. 118, 7416 (1996).
[45] Wang C, Kilitziraki M, MacBride J.A.H, Bryce M.R, Horsburgh L.E, Sheridan A.K, Monkman A.P, Samuel I.D.W, Adv. Mater. 12, 217 (2000).
[46] Murali M.G, Naveen P, Udayakumar D, Yadav V, Srivastava R, Tetrahed. Lett. 53, 157 (2012).
[47] Wang L-H, Kang E-T, Huang W, Thin Solid Films 417, 151 (2002).
[48] Sarrazin P, Beneventi D, Denneulin A, Stephan O, Chaussy D, Int. J. Polym. Sci. 2010, 1 (2010).
[49] Nguyen T-Q, Doan V, Schwartz B.J, J. Chem. Phys. 110, 4068 (1999).
[50] Catellani M, Luzzati S, Lupsac N-O, Mendichi R, Consonni R, Famulari A, Meille S.V, F Giacalone, Segura J.L, Martín N, J. Mater. Chem. 14, 67 (2004).
[51] Champion R.D, Cheng K.F, Pai C-L, Chen W-C, Jenekhe S.A, Macromol. Rapid. Commun. 26, 1835 (2005).
[52] Yu W.L, Meng H, Pei J, Huang W, J. Am. Chem. Soc.120, 11808 (1998).
[53] Huang W, Meng H, Pei J, Chen Z, Lai Y, Macromol. 32, 118 (1999).
[54] Ng S.C., Ding M, Chan H.S.O, Yu W-L, Macromol. Chem. Phys. 202, 8 (2001).
[55] Tanese M.C, Farinola G.M, Pignataro B, Valli L, Giotta L, Conoci S, Lang P, Colangiuli D, Babudri F, Naso F, Sabbatini L, Zambonin P.G, Torsi L, Chem. Mater. 18, 778 (2006).

[56] Santos Silva H, Nogueira S.L, Manzoli J.E, Barbosa Neto N.M, Marletta A, Serein-Spirau F, Lère-Porte J.-P Sandrine Lois, Silva, R.A, J. Phys. Chem. A. 115, 8288 (2011).
[57] Lois S, Florès J-C, Lère-Porte J-P, Spirau F.S, Moreau J.J.E, Miqueu K, Sotiropoulos J-M, Baylère P, Tillard M, Belin C, Eur. J. Org. Chem. 2007, 4019 (2007).
[58] Watkins N.J, Mäkinen A.J, Gao Y, Uchida M, Kafafi Z.H (2004) "Direct observation of the evolution of both the HOMO and LUMO energy levels of a silole derivative at a magnesium/silole interface". Organic Light-Emitting Materials and Devices VII, edited by Zakya H. Kafafi, Paul A. Lane, Proceedings of SPIE Vol. 5214 (SPIE, Bellingham, WA, Doi: 10.1117/12.515300
[59] Yan L, Gao Y, Thin Solid Films 417, 101 (2002).
[60] J. C. Bernède, A. Godoy, L. Cattin, F. R. Diaz, M. Morsli and M. A. del Valle (2010) in Solar Energy, Book edited by: Radu D. Rugescu, , pp. 432, INTECH, Croatia, downloaded from SCIYO.COM, Organic Solar Cells Performances Improvement Induced by Interface Buffer Layers, ISBN 978-953-307-052-0.
[61] Herbert M, Angew. Chem. Int. Ed. 44, 2482 (2005).
[62] Kanibolotsky A.L, Perepichka I.F, Skabara P.J, Chem. Soc. Rev., 39, 2695 (2010).
[63] Wallace J.U, Chen S.H, Adv. Polym. Sci. 212, 145 (2008).
[64] Chen P, Lalancette R.A, Jäkle, F, J. Am. Chem. Soc. 133, 8802 (2011).
[65] Lehnherr D, Tykwinski R.R, Aust. J. Chem. 64, 919 (2011).
[66] Pai C-L, Liu C-L, Chen W-C, Jenekhe S.A, Polym. 47, 699 (2006).
[67] Ayachi S, Ghomrasni S, Bouachrine M, Hamidi M, Alimi K, J. Mol. Str (2012, In Press)
[68] Yang L, Liao Y, Feng J-K, Ren A-M, J. Phys. Chem. A. 109, 7764 (2005).
[69] Yang L, Feng J-K, Ren A-M, J. Org. Chem. 70, 5987 (2005).
[70] Yang L, Ren A-M, Feng J-K, Wang J-F, J. Org. Chem. 70, 3009 (2005).
[71] Yang L, Feng J.K, Ren A.M, Sun C.C, Polym. 47, 3229 (2006).
[72] Yang G, Su T, Shi S, Su Z, Zhang H, Wang Y, J. Phys. Chem. A. 111, 2739 (2007).
[73] Telesca R, Bolink H, Yunoki S. Hadziioannou G. Van Duijnen P. Th, Snijders J.G, Jonkman H.T, Sawatzky G.A, Phys. Rev. B 63, 155112 (2001).
[74] Ayachi S, Alimi K, Bouachrine M, Hamidi M, Mevellec J.Y Lère-Porte J.P, Synth. Met. 156, 318 (2006).
[75] Bouachrine M, Bouzakraoui S, Hamidi M, Ayachi S, Alimi K, Lère-Porte J-P, Moreau J, Synth. Met. 145, 237 (2004).
[76] Brabec CJ, Dyakonov V, Parisi J, Sariciftci NS (2003) Organic Photovoltaics: Concepts and Realization Eds. 60, Springer, Berlin Heidelberg, pp. 169-177.
[77] Dennler G, Scharber M.C, Brabec C, Adv. Mater. 21, 1323 (2009).
[78] Wu Z, Fan B, Xue F, Adachi C, Ouyang J, Solar Energy Materials & Solar Cells 94, 2230 (2010).
[79] Al-Ibrahim M, Roth H.K, Schroedner M, Konkin A, Zhokhavets U, Gobsch G, Scharff P, Sensfuss S, Org. Electron. 6, 65 (2005).
[80] Chemek M, Wéry J, Bouachrine M, Paris M, Lefrant S, Alimi K, Synth. Met. 160, 2306 (2010).
[81] Yang Y, Zhou Y, He Q, He C, Yang C, Bai F, Li Y, J. Phys. Chem. B 113, 7745 (2009).
[82] Soci C, Hwang I, Moses D, Zhu Z, Waller D, Gaudiana R, Brabec C. J, Heeger A. J, Adv. Func. Mat. 17, 632 (2007).
[83] Huang J, Li C, Xia Y, Zhu X, Peng J, Cao Y, J. Org. Chem. 72, 8580 (2007).

[84] Colladet K, Fourier S, Cleij T.J, Lutsen L, Gelan J, Vanderzande D, Macromol. 40, 65 (2007).
[85] Roncali J, Leriche P, Cravino A, Adv. Mater. 19, 2045 (2007).
[86] Morvillo P, Bobeico E, Sol. Ener. Mat. Sol. Cells 92, 1192 (2008).
[87] Li J.C, Meng Q.B, Kim J.S, Lee Y.S, Bull. Korean Chem. Soc. 30, 951 (2009).
[88] Hou Q, Xu Y, Yang W, Yuan M, Peng J, Cao Y, J. Mater. Chem. 12, 2887 (2002).
[89] Svensson M, Zhang F, Veenstra S.C, Verhees W.J.H, Hummelen J.C, Kroon J.M, Inganäs O, Andersson M.R, Adv. Mater. 15, 988 (2003).
[90] Wu M.C, Lin Y.Y, Chen S, Liao H.C, Wu Y.J, Chen C.W, Chen Y.F, Su W.F, Chem. Phys. Lett. 468, 64 (2009).
[91] Frisch M.J, Trucks G.W, Schlegel H.B, Scuseria G.E, Robb M.A, Cheeseman J.R, Montgomery J.A, Vreven T, Kudin K.N, Burant J.C, Millam J.M, Iyengar S.S, Tomasi J, Barone V, Mennucci B, Cossi M, Scalmani G, Rega N, Petersson G.A, Nakatsuji H, Hada M, Ehara M, Toyota K, Fukuda R, Hasegawa J, Ishida M, Nakajima T, Honda Y, Kitao O, Nakai H, Klene M, Li X, Knox J.E, Hratchian H.P, Cross J.B, Adamo C, Jaramillo J, Gomperts R, Stratmann RE, Yazyev O, Austin A.J, Cammi R, Pomelli C, Ochterski J.W, Ayala P.Y, Morokuma K, Voth G.A, Salvador P, Dannenberg J.J, Zakrzewski V.G, Dapprich S, Daniels A.D, Strain M.C, Farkas O, Malick D.K, Rabuck A.D, Raghavachari K, Foresman J.B, Ortiz J.V, Cui Q, Baboul A.G, Clifford S, Cioslowski J, Stefanov B.B, Liu G, Liashenko A, Piskorz P, Komaromi I, Martin R.L, Fox D.J, Keith T, Al-Laham M.A, Peng C.Y, Nanayakkara A, Challacombe M, Gill P.M.W, Johnson B, Chen W, Wong M.W, Gonzalez C, Pople J.A, Gaussian, Inc., Pittsburgh PA, 2003.
[92] Becke AD, J. Chem. Phys. 98, 1372 (1993).
[93] Lee C, Yang W, Parr R.G, Phys. Rev. B. 37, 785 (1988).
[94] Belletête M, Beaypré S, Bouchard J, Blondin P, Leclerc M, Durocher G, J. Phys. Chem. B. 104, 9118 (2000).
[95] Matsuzawa N.N, Ishitani A, Doxon D.A, Uda T, J. Phys. Chem. A. 105, 4953 (2001).
[96] Broo A, Zerner MC, Chem. Phys. Lett. 227, 551 (1994).
[97] Sun L, Bai F.Q, Zhao Z.X, Zhang H.X, Sol. Ener. Mat & Sol. Cell. 95, 1800 (2011).
[98] Gorelsky S.I, SWizard program, University of Ottawa, Ottawa, Canada, 2009. http://www.sg-chem.net/
[99] Gorelsky S.I, Lever A.B.P, J. Organometal. Chem. 635, 187 (2001).
[100] Yang L, Ren A.M, Feng J.K, Liu X.J, Ma Y.G, Zhang M, Liu X.D, Shen J.C and Zhang HX, J. Phys. Chem. 108, 6797 (2004).
[101] Ayachi S, Ghomrasni S, Alimi K, J. App. Polym. Sci. 123, 2684 (2012).
[102] Stewart J.J.P, MOPAC 2000 Manual; Fujitsu Ltd.: Tokyo, Japan, 1999.
[103] Botta C, Destri S, Porzio W, Rossi L, Tubino R, Synth. Met. 95, 53 (1998).
[104] Lin V, Grasselli J.G, Colthup N.B (1989) Handbook of Infrared and Raman Characteristics Frequencies of Organic Molecules; Academic Press, Harcourt Brace Jovanovich Publishers: New York.
[105] Ip J, Nguen T.P, Le Rendu P, Tran V.H, Synth. Met. 122, 45 (2001).
[106] Murali M.G, Naveen P, Udayakumar D, Yadav V, Srivastava R, Tetrahed. Lett. 53, 157 (2012).
[107] Fukuda M, Sawada K, Yoshino K, J. Polym. Sci., Part A: Polym. Chem. 31, 2465 (1993).
[108] Meille S.V, Farina A, Bezziccheri F, Gallazzi M.C, Adv. Mat. 6, 848 (1994).

[109] DiCésare N, Belletête M, Leclerc M, Durocher G, J. Mol Struct: THEOCHEM. 467, 259 (1999).
[110] Leriche P, Frère P, Roncali J, J. Mater. Chem. 15, 3473 (2005).
[111] Savitha G, Hergué N, Guilmet E, Allain M, Frère P, Tetrahed. Lett. 52, 1288 (2011).
[112] Clarke T. M, Gordon K. C, Officer D. L, Hall S. B, Collis G. E, Burrell A. K, J. Phys. Chem. A. 107, 11505 (2003).
[113] Yang L, Feng J.K, Ren A.M, Polym. 46, 10970 (2005).
[114] Yang L, Feng J.K, Liao Y, Ren A.M, Opt. Mat. 29, 642 (2007).
[115] Irving D.L, Devine B.D, Sinnott S.B, J. Lumin. 126, 278 (2007).
[116] Casanovas J, Zanuy D, Aleman C, Polym. 46, 9452 (2005).
[117] Wu P-T, Kim, F.S, Champion R.D, Jenekhe S.A, Macromol. 41, 7021 (2008).
[118] May, V, Kühn O (2000) Charge and energy transfer dynamics in molecular system, Wiley-VCH, Berlin.
[119] Bouzakraoui S, Bouzzine S.M, Bouachrine M, Hamidi M, J. Mol. Struct. (THEOCHEM) 725, 39 (2005).
[120] Cao H, Ma J, Zhang G.L, Jiang Y.S, Macromol. 38, 1123 (2005).
[121] Lee Y, Russell T.P, Jo W.H, Org. Elec. 11, 846 (2010).
[122] Yang L, Feng J.K, Ren A.M, Sun C.C, Polym. 47, 3229 (2006).
[123] Koster L.J.A, Mihailetchi V.D, Blom P.W, Appl. Phys. Lett. 88, 093511 (2006).
[124] Kato S, Matsumoto T, Shigeiwa M, Gorohmaru H, Maeda S, Ishi-i T, Mataka S, Chem. Eur. J. 12, 2303 (2006).
[125] Wei H, Scudiero L, Eilers H, Appl. Surf. Sci. 255, 8593 (2009).
[126] Mabrouk A, Alimi K, Hamidi M, Bouachrine M, Molinie P, Polym. 46, 9928 (2005).
[127] Chen J.W, Cao Y, Acc. Chem. Res. 42, 1709 (2009).
[128] Rong Z.C, Jiang L.Z, Hong C.Y, Shan C.H, Zhi W.Y, Hua Y.L, J. Mol. Str. THEOCHEM 899, 86 (2009).
[129] He Y, Chen H.Y, Hou J.H, Li Y.F, J. Am. Chem. Soc. 132, 1377 (2010).
[130] Kooistra F.B, Knol J, Kastenberg F, Popescu L.M, Verhees W.J.H, Kroon J.M, Hummelen J.C, Org. Lett. 9, 551 (2007).
[131] Gadisa A, Svensson M, Andersson M.R, Inganas O, Appl. Phys. Lett. 84, 1609 (2004).
[132] Mühlbacher D, Scharber M, Morana M, Zhu Z, Waller D, Gaudiana R, Brabec C, Adv. Mater. 18, 2884 (2006).
[133] Brabec C.J, Cravino A, Meissner D, Sariciftci N.S, Fromherz T, Rispens M.T, Sanchez L, Hummelen J.C, Adv. Funct. Mater. 11, 374 (2001).
[134] Gûnes S, Neugebauer H, Sariciftci N.S, Chem. Rev. 107, 1324 (2007).
[135] Liu J, Shi Y, Yang Y, Adv. Funct. Mat. 11, 420 (2001).
[136] Scharber M.C, Mühlbacher D, Koppe M, Denk P, Waldauf C, Heeger A.J, Barbec C.J, Adv. Mater. 18,789 (2006).